

N 62 54954

**CASE FILE  
COPY**

**NATIONAL ADVISORY COMMITTEE  
FOR AERONAUTICS**

**TECHNICAL NOTE 2954**

THE STRUCTURE OF TURBULENCE IN FULLY  
DEVELOPED PIPE FLOW

By John Laufer

National Bureau of Standards



Washington

June 1953

1953 N T 2954

TN 2954

NATIONAL ADVISORY COMMITTEE FOR AERONAUTICS

TECHNICAL NOTE 2954

THE STRUCTURE OF TURBULENCE IN FULLY  
DEVELOPED PIPE FLOW

By John Laufer

SUMMARY

Measurements, principally with a hot-wire anemometer, were made in fully developed turbulent flow in a 10-inch pipe at speeds of approximately 10 and 100 feet per second. Emphasis was placed on turbulence and conditions near the wall. The results include relevant mean and statistical quantities, such as Reynolds stresses, triple correlations, turbulent dissipation, and energy spectra. It is shown that rates of turbulent-energy production, dissipation, and diffusion have sharp maximums near the edge of the laminar sublayer and that there exist a strong movement of kinetic energy away from this point and an equally strong movement of pressure energy toward it. Finally it is suggested that, from the standpoint of turbulent structure, the field may be divided into three regions: (1) Wall proximity where turbulence production, diffusion, and viscous action are all of about equal importance; (2) the central region of the pipe where energy diffusion plays the predominant role; and (3) the region between (1) and (2) where the local rate of change of turbulent-energy production dominates the energy received by diffusive action.

INTRODUCTION

The one aspect of turbulent shear flow that stands out most prominently is the transport of stream properties by turbulent motions. The transfer process is fundamental, for it not only shapes the mean-flow field through momentum transfer but supplies the mechanism by which turbulent motions receive energy from the mean-flow field. The well-known phenomenological theories were the first attempts to give analytical forms for the transfer mechanism by some simple physical considerations and thereby succeeded in making predictions about the nature of the mean-velocity field. Subsequent experiments, however, have clearly demonstrated the inadequacies of these theories, and in a systematic discussion Batchelor (ref. 1) has pointed out the inconsistencies and unreal consequences of the assumptions involved. Recently, Rotta (ref. 2) and Tchen (ref. 3) presented more extensive and deeper analytical treatments of the nonisotropic turbulence problem, and, although

their results show some agreement with the existing experimental findings, they cannot escape some arbitrariness in assuming the nature of the transfer mechanism. It is the general opinion among investigators in this field that more extensive experimental work on the turbulence mechanism is necessary before a satisfactory analytical formulation of the problem will be possible.

In the last few years various experimental investigations were carried out in different types of shear flows. It became apparent that the dynamic and kinematic processes governing such flows may be quite different. The difference between the so-called free turbulent flows and flows past solid boundaries has recently been emphasized by the phenomenon of intermittency, first noted in a jet by Corrsin (ref. 4) and later more clearly recognized and studied in detail in the wake of a cylinder by Townsend (ref. 5). It is apparent by now that in flows like wakes, jets, and those near the free surface of the boundary layers the intermittency is present and seems to play a very important role in the transfer mechanism, while in pipe and channel flows it is completely absent.

Fairly large amounts of experimental information have been gathered about flows with free boundaries (refs. 6, 7, and 8); especially extensive is the work by Townsend in a turbulent wake (ref. 5). The recent work in two-dimensional channel flow by the present writer (ref. 9) brought out some significant features of flows with solid boundaries, but the information was far from being complete. One consequence of this study was the realization that in order to obtain a complete picture, say of the turbulent-energy balance, a knowledge of flow conditions in close proximity to the wall was of utmost importance.

Since no similar investigation, with emphasis on the turbulent structure, has ever been carried out in fully developed pipe flow, the present investigation was undertaken. A pipe also offered the simplicity of axially symmetric mean flow and a turbulent field nonhomogeneous in one direction only. At the same time it afforded an experimentally convenient setup for obtaining a shear flow of large scale. A diameter of 10 inches was chosen as sufficiently large for the favorable application of hot-wires and for bringing the region near the wall within practical reach. To cover the desired range, two working Reynolds numbers were chosen, these being 500,000, based on the diameter and an airspeed at the center of 100 feet per second, and 50,000 at a speed of 10 feet per second. The higher Reynolds number minimized viscous effects while the lower one magnified the extent of the predominantly viscous layer near the wall. This turned out to be a fortunate choice since experimental difficulties and errors encountered in one case were usually absent in the other.

The purpose was to investigate the nature of turbulence and its relation to the mean flow, in particular the rates of transfer,

diffusion, and dissipation of energy. To this end measurements were made of the relevant mean and statistical quantities, including their spatial distributions from within the laminar sublayer to the center and energy spectra at several radii. Thus the purpose was to reveal details of flow structure that could not be found from studies of mean flow alone, and yet stop short of a direct attempt to find the nature of the transfer mechanism. It is hoped, however, that advances toward the latter goal will have been made through the present work.

The present investigation was conducted under the sponsorship and with the financial assistance of the National Advisory Committee for Aeronautics. The author wishes to express his gratitude to Dr. G. B. Schubauer for his constant interest and encouragement throughout this work. The valuable discussions with Dr. C. M. Tchen and Mr. P. S. Klebanoff are also much appreciated. Thanks are due to Miss Z. W. Diehl and Mr. K. D. Tidstrom who carried out the numerical computations and preparation of the report.

## SYMBOLS

$a$  pipe radius, 4.86 in.

$D_o, D_T$  dimensionless turbulent-kinetic-energy diffusion

$$\text{rates; } D_o \equiv \frac{a}{U_T^3} \frac{1}{r} \frac{d}{dr} r v \overline{\left( \frac{u^2 + v^2 + w^2}{2} \right)},$$

$$D_T \equiv \frac{v}{U_T^4} \frac{1}{r} \frac{d}{dr} r v \overline{\left( \frac{u^2 + v^2 + w^2}{2} \right)}$$

$e_1, e_2$  voltage fluctuations across hot-wires

$F_u(k_1)$  fraction of turbulent energy  $\overline{u^2}$  associated with  $k_1$ ,  
cm<sup>3</sup>/sec<sup>2</sup>

$F_v(k_1)$  fraction of turbulent energy  $\overline{v^2}$  associated with  $k_1$ ,  
cm<sup>3</sup>/sec<sup>2</sup>

$F_w(k_1)$  fraction of turbulent energy  $\overline{w^2}$  associated with  $k_1$ ,  
cm<sup>3</sup>/sec<sup>2</sup>

$(GD)_\tau$	dimensionless gradient diffusion rate of turbulent kinetic energy, $\frac{\nu^2}{U_\tau^4} \frac{1}{r} \frac{d}{dr} r \frac{d}{dr} \frac{u^2 + v^2 + w^2}{2}$
$k_1$	one-dimensional wave number in direction of mean flow, $\text{cm}^{-1}$
$P$	mean pressure at any point in pipe
$P_e$	mean pressure at exit of pipe
$(PD)_o, (PD)_\tau$	dimensionless turbulent-pressure-energy diffusion rates; $(PD)_o \equiv \frac{a}{U_\tau^3} \frac{1}{r} \frac{d}{dr} r \overline{vp}$ , $(PD)_\tau \equiv \frac{\nu}{U_\tau^4} \frac{1}{r} \frac{d}{dr} r \overline{vp}$
$(Pr)_o, (Pr)_\tau$	dimensionless turbulent-energy production rates; $(Pr)_o \equiv a \frac{\overline{uv}}{U_\tau^3} \frac{dU}{dr}$ , $(Pr)_\tau \equiv \nu \frac{\overline{uv}}{U_\tau^4} \frac{dU}{dr}$
$p$	instantaneous value of pressure fluctuations
$q$	dynamic pressure at pipe center
$R$	Reynolds number based on diameter of pipe and velocity at pipe center
$R_r$	correlation coefficient of u-fluctuations at two points displaced in a radial direction
$r$	coordinate in radial direction; $r = 0$ corresponds to pipe center
$r' \equiv a - r$	
$r^*$	friction distance parameter, $r'U_\tau/\nu$
$t$	time
$U$	mean velocity at any point in pipe
$U_o$	maximum value of mean velocity

$U_\tau$	friction velocity; $U_\tau^2 \equiv -v \left( \frac{dU}{dr} \right)_{r=a}$
$u_1, u_2, u_3$	total (mean-plus-fluctuating) velocities in x, r, and $\phi$ directions, respectively
$u, v, w$	instantaneous values of velocity fluctuations in x, r, and $\phi$ directions, respectively
$u', v', w'$	root-mean-square values of velocity fluctuations in x, r, and $\phi$ directions, respectively
$V, W$	mean velocities in radial and azimuthal direction, respectively
$W_0, W_\tau$	dimensionless turbulent-energy dissipation rates; $W_0 \equiv a \frac{v}{U_\tau^3} \overline{\left( \frac{\partial u_i}{\partial x_j} \right) \left( \frac{\partial u_i}{\partial x_j} \right)}, \quad W_\tau \equiv \frac{v^2}{U_\tau^4} \overline{\left( \frac{\partial u_i}{\partial x_j} \right) \left( \frac{\partial u_i}{\partial x_j} \right)}$ where $u_i$ refers to three velocity fluctuation components u, v, and w and $x_j$ , to three coordinates; repeated indices indicate summation
$W_\mu$	dimensionless direct-viscous-dissipation rate, $\frac{v^2}{U_\tau^4} \left( \frac{dU}{dr} \right)^2$
$\lambda$	dissipation length parameter
$\nu$	kinematic viscosity of air
$\pi$	total (mean-plus-fluctuating) pressure
$\rho$	air density
$\phi$	azimuthal coordinate

## ANALYTICAL CONSIDERATIONS

## Equations of Motion of Pipe Flow

The continuity equation and Reynolds equation in cylindrical coordinates for incompressible mean flow have the following form:

$$\frac{\partial U}{\partial x} + \frac{1}{r} \frac{\partial rV}{\partial r} + \frac{1}{r} \frac{\partial W}{\partial \phi} = 0 \quad (1)$$

and

$$\left. \begin{aligned} U \frac{\partial U}{\partial x} + V \frac{\partial U}{\partial r} + \frac{W}{r} \frac{\partial U}{\partial \phi} &= -\frac{1}{\rho} \frac{\partial P}{\partial x} - \left( \frac{\partial}{\partial x} \overline{u^2} + \frac{1}{r} \frac{\partial}{\partial r} r \overline{uv} + \frac{1}{r} \frac{\partial}{\partial \phi} \overline{uw} \right) + \nu \nabla^2 U \\ U \frac{\partial V}{\partial x} + V \frac{\partial V}{\partial r} + \frac{W}{r} \frac{\partial V}{\partial \phi} - \frac{W^2}{r} &= -\frac{1}{\rho} \frac{\partial P}{\partial r} - \left( \frac{\partial}{\partial x} \overline{uv} + \frac{1}{r} \frac{\partial}{\partial r} r \overline{v^2} + \right. \\ \left. \frac{1}{r} \frac{\partial}{\partial \phi} \overline{vw} - \frac{\overline{W^2}}{r} \right) &+ \nu \left( \nabla^2 V - \frac{V}{r^2} - \frac{2}{r^2} \frac{\partial W}{\partial \phi} \right) \\ U \frac{\partial W}{\partial x} + V \frac{\partial W}{\partial r} + \frac{W}{r} \frac{\partial W}{\partial \phi} - \frac{VW}{r} &= -\frac{1}{\rho r} \frac{\partial P}{\partial \phi} - \left( \frac{\partial}{\partial x} \overline{uw} + \right. \\ \left. \frac{\partial}{\partial r} \overline{vw} + \frac{1}{r} \frac{\partial}{\partial \phi} \overline{w^2} - \frac{2\overline{vw}}{r} \right) &+ \nu \left( \nabla^2 W + \frac{2}{r^2} \frac{\partial W}{\partial \phi} - \frac{W}{r^2} \right) \end{aligned} \right\} (2)$$

where

$$\nabla^2 = \frac{\partial^2}{\partial x^2} + \frac{\partial^2}{\partial r^2} + \frac{1}{r} \frac{\partial}{\partial r} + \frac{1}{r^2} \frac{\partial^2}{\partial \phi^2}$$

In a fully developed turbulent pipe flow the conditions are

$$(a) \quad V = 0 \quad \text{and} \quad W = 0$$

$$(b) \quad \frac{\partial}{\partial \varphi} = 0$$

(c) The velocity field is independent of the coordinate  $x$

Equations (2) therefore become

$$\frac{1}{\rho} \frac{\partial P}{\partial x} = -\frac{1}{r} \frac{d}{dr} r \overline{uv} + \nu \left( \frac{d^2 U}{dr^2} + \frac{1}{r} \frac{dU}{dr} \right)$$

$$\frac{1}{\rho} \frac{\partial P}{\partial r} = -\frac{1}{r} \frac{d}{dr} r \overline{v^2} + \frac{\overline{w^2}}{r}$$

$$0 = -\frac{d}{dr} \overline{vw} - \frac{2\overline{vw}}{r}$$

Integrating the last equation and using the boundary condition  $\overline{vw} = 0$  at  $r = a$  it follows that  $\overline{vw} = 0$  for all values of  $r$ . Thus the Reynolds equations for the turbulent pipe flow reduce to

$$\frac{1}{\rho} \frac{\partial P}{\partial x} = -\frac{1}{r} \frac{d}{dr} r \left( \overline{uv} - \nu \frac{dU}{dr} \right) \quad (3a)$$

$$\frac{1}{\rho} \frac{\partial P}{\partial r} = -\frac{1}{r} \frac{d}{dr} r \overline{v^2} + \frac{\overline{w^2}}{r} \quad (3b)$$

Differentiating equation (3b) with respect to  $x$  one finds  $\partial^2 P / \partial r \partial x = 0$ . Thus  $\partial P / \partial x$  is independent of  $r$  and equations (3a) and (3b) readily integrate to

$$\frac{r^2}{2} \frac{1}{\rho} \frac{\partial P}{\partial x} = -r \left( \overline{uv} - \nu \frac{dU}{dr} \right) + A(x) \quad (4a)$$

$$\frac{P}{\rho} = -\overline{v^2} + \int_a^r \frac{\overline{w^2} - \overline{v^2}}{r} dr + B(x) \quad (4b)$$

The boundary conditions are at  $r = 0$

$$\overline{uv} = 0$$

$$\frac{dU}{dr} = 0$$

and at  $r = a$

$$\overline{uv} = 0$$

$$v \frac{dU}{dr} = -U_T^2$$

$$\overline{v^2} = 0$$

Also let  $P = 0$  at  $x = 0$  and  $r = a$ . Then from equation (4a),  $A(x) = 0$ ,

$$\frac{1}{\rho} \frac{\partial P}{\partial x} = -\frac{2}{a} U_T^2$$

and, integrating,

$$\frac{P}{\rho} = -\frac{2}{a} U_T^2 x + C(r) \quad (5)$$

From equations (4b) and (5),  $B(x) = -\frac{2}{a} U_T^2 x$ . The equations finally become

$$\overline{uv} = v \frac{dU}{dr} + \frac{r}{a} U_T^2 \quad (6a)$$

$$\overline{v^2} + \int_a^r \frac{\overline{v^2} - \overline{w^2}}{r} dr = -\frac{P}{\rho} - \frac{2}{a} U_T^2 x \quad (6b)$$

It is interesting to note, as already pointed out by Kampé de Fériet in the case of flows between parallel walls (ref. 10), that the shearing stress  $\overline{uv}$  and the mean velocity occur together in one equation and the normal stresses  $\overline{v^2}$  and  $\overline{w^2}$  and the mean pressure occur together in the other. From the experimental point of view this has the advantage that the equations furnish a method of checking the absolute accuracy of the measurements of the Reynolds stresses if the mean-velocity and pressure distributions are known.

Energy Equations

The momentum equations may be written in the form

$$\left. \begin{aligned} \frac{\partial u_1^2}{\partial x} + \frac{\partial u_1 u_2}{\partial r} + \frac{1}{r} \frac{\partial u_1 u_3}{\partial \phi} + \frac{u_1 u_2}{r} &= -\frac{1}{\rho} \frac{\partial \pi}{\partial x} + \nu \nabla^2 u_1 \\ \frac{\partial u_1 u_2}{\partial x} + \frac{\partial u_2^2}{\partial r} + \frac{1}{r} \frac{\partial u_2 u_3}{\partial \phi} + \frac{u_2^2 - u_3^2}{r} &= -\frac{1}{\rho} \frac{\partial \pi}{\partial r} + \nu \left( \nabla^2 u_2 - \frac{u_2}{r^2} - \frac{2}{r^2} \frac{\partial u_3}{\partial \phi} \right) \\ \frac{\partial u_1 u_3}{\partial x} + \frac{\partial u_2 u_3}{\partial r} + \frac{1}{r} \frac{\partial u_3^2}{\partial \phi} - \frac{2u_2 u_3}{r} &= -\frac{1}{\rho r} \frac{\partial \pi}{\partial \phi} + \nu \left( \nabla^2 u_3 - \frac{u_3}{r^2} + \frac{2}{r^2} \frac{\partial u_3}{\partial \phi} \right) \end{aligned} \right\} (7)$$

Multiplying the three equations by  $u_1$ ,  $u_2$ , and  $u_3$ , respectively, one gets

$$\begin{aligned} \frac{\partial u_1^3}{\partial x} + \frac{\partial u_1^2 u_2}{\partial r} + \frac{1}{r} \frac{\partial u_1^2 u_3}{\partial \phi} + \frac{u_1^2 u_2}{r} &= -\frac{2}{\rho} u_1 \frac{\partial \pi}{\partial x} + \\ &2\nu \left[ \frac{1}{2} \nabla^2 u_1^2 - \left( \frac{\partial u_1}{\partial x} \right)^2 - \left( \frac{\partial u_1}{\partial r} \right)^2 - \frac{1}{r^2} \left( \frac{\partial u_1}{\partial \phi} \right)^2 \right] \\ \frac{\partial u_1 u_2^2}{\partial x} + \frac{\partial u_2^3}{\partial r} + \frac{1}{r} \frac{\partial u_2^2 u_3}{\partial \phi} + \frac{u_2(u_2^2 - u_3^2)}{r} &= -\frac{2}{\rho} u_2 \frac{\partial \pi}{\partial r} + \\ &2\nu \left[ \frac{1}{2} \nabla^2 u_2^2 - \left( \frac{\partial u_2}{\partial x} \right)^2 - \left( \frac{\partial u_2}{\partial r} \right)^2 - \frac{1}{r^2} \left( \frac{\partial u_2}{\partial \phi} \right)^2 - \frac{u_2^2}{r^2} - \frac{2}{r^2} u_2 \frac{\partial u_3}{\partial \phi} \right] \\ \frac{\partial u_1 u_3^2}{\partial x} + \frac{\partial u_2 u_3^2}{\partial r} + \frac{1}{r} \frac{\partial u_3^3}{\partial \phi} + \frac{2u_2 u_3^2}{r} &= -\frac{2}{\rho} \frac{u_3}{r} \frac{\partial \pi}{\partial \phi} + \\ &2\nu \left[ \frac{1}{2} \nabla^2 u_3^2 - \left( \frac{\partial u_3}{\partial x} \right)^2 - \left( \frac{\partial u_3}{\partial r} \right)^2 - \frac{1}{r^2} \left( \frac{\partial u_3}{\partial \phi} \right)^2 - \frac{u_3^2}{r^2} + \frac{2}{r^2} u_3 \frac{\partial u_3}{\partial \phi} \right] \end{aligned}$$

Introducing the velocity and pressure perturbations

$$u_1 = U + u$$

$$u_2 = v$$

$$u_3 = w$$

$$\pi = P + p$$

averaging, and adding the three equations there is obtained the energy equation for the turbulent motion

$$\begin{aligned} \overline{uv} \frac{dU}{dr} + \frac{1}{r} \frac{d}{dr} r v \overline{\left( \frac{u^2 + v^2 + w^2}{2} + \frac{p}{\rho} \right)} = \\ \frac{v}{r} \frac{d}{dr} r \frac{d}{dr} \overline{\frac{u^2 + v^2 + w^2}{2}} + \frac{v}{r} \left( \frac{4}{r} \overline{w \frac{\partial v}{\partial \phi}} - \frac{v^2 + w^2}{r} \right) - v \overline{\left( \frac{\partial u_i}{\partial x_j} \right) \left( \frac{\partial u_i}{\partial x_j} \right)} \end{aligned} \quad (8)$$

where in the last term  $u_i$  refers to the three velocity fluctuation components and  $x_j$ , to the three coordinates; the repeated indices indicate summation.

The second term on the right-hand side of the equation may be neglected compared with the other terms for all values of  $r$ , since (a) near the center it approaches zero as  $r \rightarrow 0$  as may be shown from the continuity equation; and (b) everywhere else its order of magnitude  $\overline{vu^2}/D^2$ , where  $D$  is a characteristic length of the order of the pipe radius, is smaller than, for instance, that of the last term of the equation; that is,  $\overline{vu^2}/\lambda^2 \gg \overline{vu^2}/D^2$ , since  $\lambda^2/D^2 \ll 1$ .

The equation may now be rewritten as

$$\begin{aligned} \overline{uv} \frac{dU}{dr} + \frac{1}{r} \frac{d}{dr} r v \overline{\left( \frac{u^2 + v^2 + w^2}{2} + \frac{p}{\rho} \right)} - \\ \frac{v}{r} \frac{d}{dr} r \frac{d}{dr} \overline{\frac{u^2 + v^2 + w^2}{2}} + v \overline{\left( \frac{\partial u_i}{\partial x_j} \right) \left( \frac{\partial u_i}{\partial x_j} \right)} = 0 \end{aligned} \quad (9)$$

The energy equation thus obtained has essentially the same form as that given by Von Kármán for the case of a turbulent flow between two parallel plates (ref. 11). The first term corresponds to the rate of production of turbulent energy by the action of the shearing stresses. The second term represents the rate of energy change due to transfer of both kinetic and potential energies by the radial velocity fluctuations and is usually referred to as the diffusion term. The third expression may be regarded as a gradient type of energy diffusion and is important only very near the wall. The fourth term expresses the rate of energy dissipation into heat by action of the viscosity.

## EQUIPMENT

### Wind Tunnel

The investigation was carried out in the experimental setup shown in figure 1. A centrifugal blower having a capacity of 12,000 cubic feet per minute and powered by a 15-horsepower constant-speed motor was placed inside a large pressure box. The box was octagonal in cross section and was 10 feet high and 16 feet long. The air was discharged from the blower into the space surrounding the blower and then passed through a honeycomb, three screens, and a large contraction cone. The honeycomb consisted of hexagonal cells 2 inches across and 8 inches long. The screens had 24 meshes per inch and a wire diameter of 0.0075 inch. The contraction cone, which was made out of hardwood and was circular in cross section, reduced the air passage from 48 inches to 18 inches in diameter. The cross section was then further reduced from 18 inches to 10 inches in diameter through a 90° elbow. After the elbow a short elastic coupling was used to prevent the transmission of vibration from the pressure box to the pipe. In order to minimize any flow irregularities due to the elbow, another screen and an 8-inch-long honeycomb were installed in the entrance sections of a 25-foot-long steel pipe. Furthermore, in order to accelerate the boundary-layer growth, the pipe wall was artificially roughened by gluing floor-sanding paper to the surface along a length of  $2\frac{1}{2}$  feet. With this arrangement it was found from the measured mean-velocity distribution at the end of the steel pipe, that is, after an entrance length of about 30 diameters, that the flow was fully developed turbulent. Following the steel pipe, a 16-foot-long seamless brass tube was attached having an inside diameter of 9.72 inches. This served as the actual test section.

The speed of the tunnel was regulated by throttling the intake of the blower with adjustable vanes and by venting the pressure box. In the early stages of the investigation it was realized that for the very low velocity pipe experiments, where the intake of the blower had to be

nearly closed, the heat dissipated in the pressure box was sufficient to affect the flow in the test section. This difficulty was overcome by supplying the air to the system by a ventilating fan placed on the side of the box as shown in figure 1.

#### Hot-Wire Equipment

The basic hot-wire equipment used during the investigation is described in detail in reference 12. The hot-wires were made of platinum drawn by the Wollaston process. Later during the investigation platinum-rhodium wires (90 percent platinum and 10 percent rhodium) were used and were found to be very satisfactory. The wire diameters were generally 0.0001 inch; only when the noise problem was very critical were finer wires (0.00005 inch) used. For the measurements of the longitudinal components of the velocity fluctuations the length of the wires ranged from 0.01 to 0.025 inch.

Special care was taken in building the X-type of wires for the measurements of the cross components  $v$  and  $w$ . In order to minimize wire-length effects and to be able to work very near the wall, the size of the wire holder had to be as small as possible. With the use of prongs made of fine jeweler's broaches the dimensions of the holder head were cut down to approximately 0.015 inch by 0.005 inch, the wires having a length about 0.025 inch.

#### Traversing Mechanism

The traversing mechanism simply consisted of a micrometer screw on which the hot-wire support was fastened. The support could be rotated in a plane perpendicular to the air flow so that the hot-wire could be adjusted parallel to the wall.

The zero reading of the traversing mechanism ( $r' = 0$ ) was found by placing the hot-wire close to the wall (approximately 0.01 inch away) and measuring the distance between the wire and its image in the polished wall by an ocular micrometer. Since the curvature of the wall was small, the space between the wire and the wall could be taken as half the observed distance.

#### PROCEDURE AND RESULTS

While fully developed turbulent flow was readily obtained throughout the 16-foot test length, tedious and time-consuming adjustments had to be made to remove secondary effects and obtain axial symmetry. The task was particularly difficult at the low Reynolds numbers where the

effect of temperature gradient was most felt. This as well as disturbances from the elbow had to be eliminated. After the final adjustments, pressure and velocity surveys made along the 16-foot test length showed that the velocity field at each section was the same and symmetry about the axis had been obtained. All the final measurements were made inside the tube 2 to 4 inches from the exit.

#### Measurement of Mean Velocity and Pressure

The experiment was conducted at two Reynolds numbers, 50,000 and 500,000, corresponding to maximum mean velocities of approximately 10 and 100 feet per second, these velocities being varied slightly in order to compensate for the daily changes in air viscosity and density. In order to cover the wide range of static and dynamic pressures, an inclined manometer 5 feet in length was used. With benzol and a slope of 10 to 1 the manometer was sensitive to 0.005 centimeter of water by direct reading. With a traveling microscope and separate scale the sensitivity was increased to 0.0001 centimeter of water.

The pressure distribution in the direction of the flow was measured through pressure taps located every 2 feet along the brass tube. The results are given in figure 2.

Small total-head and static tubes were made of 0.04-inch-diameter nickel tube stock with 0.003-inch wall thickness. The tip of the total-head tube was flattened to an opening of 0.006 inch. The static tube was placed approximately 0.4 inch above the total-head tube. This arrangement was used for measuring the complete velocity distribution in the low Reynolds number case. In the vicinity of the wall a correction had to be made because of the large level of velocity fluctuations. The correction, having the form

$$U_{\text{corr}} = U \sqrt{1 - \frac{\overline{u^2} + \overline{v^2} + \overline{w^2}}{U^2}} \approx U \sqrt{1 - \frac{\overline{u^2}}{U^2}}$$

was of the order of 5 percent or less.

For the high Reynolds number a hot-wire was used to explore the mean-velocity distribution near the wall. Here again a correction for velocity fluctuations had to be made because of the nonlinear behavior of the hot-wire. This was accomplished by an approximate graphical method using the known static response curve of the wire (voltage against velocity) and the known root-mean-square value of the voltage fluctuations. The maximum correction was about 10 percent, the correct

mean velocity being higher than the observed. At the low Reynolds number the velocity profile determined by the hot-wire was unreasonably low in the vicinity of the wall after applying the correction. Except for this, the agreement between the hot-wire results and those obtained with the total-head tube was good.

The measurements are presented in figures 3 and 4. In figure 4 the dashed lines indicate the wall velocity gradients computed from the pressure drop. The agreement with the measured values is satisfactory.

#### Measurements of Turbulence Levels and Shearing Stress

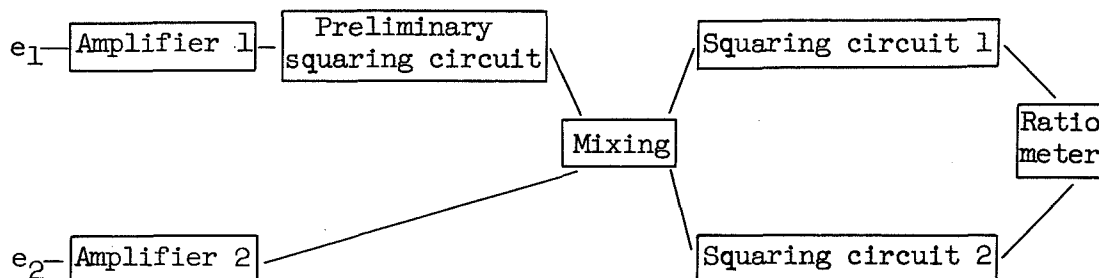
The three components of the velocity fluctuations  $u'$ ,  $v'$ , and  $w'$  and the turbulent shearing stress  $\overline{uv}$  were obtained by standard techniques described in reference 6.

Figures 5 to 8 give the detailed results. In figure 8 the solid lines represent distributions calculated by equation (6a) using the independently measured mean-velocity gradients and  $u'$  and  $v'$ . It is seen that for the high Reynolds number the agreement between these and the directly measured points is very good while for the low Reynolds number the measured points are somewhat higher. It should be mentioned that lower accuracy of all the measurements in the low Reynolds number flow is to be expected mainly because of the difficulty of forming consistent time averages because of the inherent low-frequency fluctuations.

#### Measurements of Triple and Quadruple

##### Velocity Correlations

Measurements of the triple and quadruple velocity correlations are given in figures 9, 10, and 11. The basic technique described in reference 12 was essentially adopted for these measurements. The schematic diagram of the electronic circuit is given below:



The two hot-wire signals  $e_1$  and  $e_2$  are fed into two identical compensated amplifiers after which  $e_1$  is squared. The preliminary squaring circuit uses the nonlinear characteristics of two balanced triodes as employed in Townsend's circuit (ref. 13). The output of the mixing circuit, which is a simple resistance network (ref. 12), gives simultaneously the sum and difference of the inputs. Squaring circuits 1 and 2 contain a series of diodes properly biased to give the square of the inputs. If the signals before the mixing circuit are equalized the ratio meter reads directly the correlation coefficient  $\overline{e_1^2 e_2} / \sqrt{\overline{e_1^4 e_2^2}}$ .

It is seen that in order to obtain the triple velocity correlations by this method the mean fourth power is necessary. This could have been avoided, of course, if instead of using the ratio meter the outputs of the two squaring circuits had been recorded separately and then subtracted. It was felt, however, that the method adopted gave more consistent results. The mean fourth power was obtained simply by feeding the amplified hot-wire signal into a squaring circuit and then squaring the output again by reading the final output on a thermocouple meter.

Unfortunately, for the lower Reynolds number some inconsistency in the measurements was found using the above technique. In comparing the values of the double-correlation coefficient  $\overline{uv}/u'v'$  obtained by this setup (without the preliminary squaring circuit) with those obtained by the conventional method, they were found to be from 20 percent to 30 percent lower everywhere except near the wall. At the high Reynolds number the agreement was very satisfactory. Although, because of time limitations, it was not possible to trace definitely the cause of this discrepancy, it is believed to be due to a difference in the low-frequency phase shift of the two amplifiers. Consequently, the large difference between the triple-correlation distributions at the two Reynolds numbers in figure 11 should be considered to be due to experimental error.

#### Measurements of Various Dissipation Terms

The expression for the rate of energy dissipation as it appears in the turbulent-energy equation (9) has the form

$$W = \nu \left[ \overline{\left(\frac{\partial u}{\partial x}\right)^2} + \overline{\left(\frac{\partial v}{\partial x}\right)^2} + \overline{\left(\frac{\partial w}{\partial x}\right)^2} + \overline{\left(\frac{\partial u}{\partial r}\right)^2} + \overline{\left(\frac{\partial v}{\partial r}\right)^2} + \overline{\left(\frac{\partial w}{\partial r}\right)^2} + \frac{1}{r^2} \overline{\left(\frac{\partial u}{\partial \phi}\right)^2} + \frac{1}{r^2} \overline{\left(\frac{\partial v}{\partial \phi}\right)^2} + \frac{1}{r^2} \overline{\left(\frac{\partial w}{\partial \phi}\right)^2} \right] \quad (10)$$

The first three terms were obtained by the differentiation method introduced by Townsend (ref. 13). By making the assumption

$$\frac{\partial}{\partial x} = -\frac{1}{U} \frac{\partial}{\partial t} \quad (11)$$

he writes

$$\overline{\left(\frac{\partial u}{\partial x}\right)^2} = \frac{1}{U^2} \overline{\left(\frac{\partial u}{\partial t}\right)^2}$$

Thus by electronically differentiating the hot-wire signal  $e \propto u$  (or  $v$ , or  $w$ ),  $\overline{\left(\frac{\partial u}{\partial x}\right)^2}$  may be easily obtained. A recent paper by Lin (ref. 14) shows that this assumption is valid if no mean-velocity gradient exists and  $(u/U)^2 \ll 1$ . In a shear flow he gives an additional condition

$$U \frac{\partial u}{\partial x} \gg v \frac{\partial U}{\partial r}$$

In the present measurements these conditions were found to be satisfied with the exception of a region inside the laminar sublayer. Also during the course of a boundary-layer investigation at the NBS an experimental verification of the validity of this method was made at 0.05 times the boundary-layer thickness.

The fourth and seventh terms of equation (10) were obtained essentially by a method first suggested by Taylor (ref. 15), in which

$$R_r \equiv \frac{\overline{uu(\bar{r})}}{u'u'(\bar{r})} \approx 1 - \frac{1}{2u^2} \overline{\left(\frac{\partial u}{\partial r}\right)^2} \bar{r}^2$$

as  $\bar{r} \rightarrow 0$ , where  $u$  and  $u(\bar{r})$  denote fluctuations at distance  $\bar{r}$  apart. Thus by measuring the correlation coefficient  $R_r$  for small

values of  $\bar{r}$ ,  $\overline{\left(\frac{\partial u}{\partial r}\right)^2}$  can be calculated. During the present investigation the accuracy of the method was greatly improved by adopting the following technique: The above equation may be rewritten as

$$R_r = \frac{\overline{u^2} + \overline{u^2(\bar{r})}}{2u'u'(\bar{r})} - \frac{\overline{[u - u(\bar{r})]^2}}{2u'u'(\bar{r})} \approx 1 - \frac{1}{2u^2} \overline{\left(\frac{\partial u}{\partial r}\right)^2} \bar{r}^2$$

Since, for small values of  $\bar{r}$ ,  $\overline{u^2} = \overline{u^2(\bar{r})}$ , one has

$$\sigma \equiv \frac{\overline{[u - u(\bar{r})]^2}}{2\overline{u^2}} = \frac{1}{2\overline{u^2}} \overline{\left(\frac{\partial u}{\partial r}\right)^2} \bar{r}^2$$

Several values of  $\sigma$  can be easily measured by placing two hot-wires at various small distances  $\bar{r}$  apart. Then  $\overline{\left(\frac{\partial u}{\partial r}\right)^2}$  may be calculated from the slope of a straight line in a plot of  $\sigma$  against  $\bar{r}^2$ .

The remaining four terms of equation (10) could also have been obtained with the method described above. However, the wire arrangement necessary for such a technique made its application impractical. Comparing the first three terms it was found that they satisfy the isotropic relations fairly well except near the wall (figs. 12 and 13). The other two measured terms, while not too different from the first

three in the center region, are considerably higher (especially  $\overline{\left(\frac{\partial u}{\partial r}\right)^2}$ ) near the wall. This, of course, is not surprising since dissipation lengths or microscales in the radial direction are expected to be smaller because of the presence of the wall. For want of a better procedure it was assumed that mean-square derivatives with respect to a given direction separately satisfied the isotropic relations

$$\overline{2\left(\frac{\partial v}{\partial r}\right)^2} = \overline{\left(\frac{\partial w}{\partial r}\right)^2} = \overline{\left(\frac{\partial u}{\partial r}\right)^2}$$

$$\overline{\frac{1}{r^2}\left(\frac{\partial v}{\partial \phi}\right)^2} = \overline{\frac{2}{r^2}\left(\frac{\partial w}{\partial \phi}\right)^2} = \overline{\frac{1}{r^2}\left(\frac{\partial u}{\partial \phi}\right)^2}$$

It is not possible to estimate the accuracy of this assumption at particular points. However, one can determine the error made in the total energy dissipation of the pipe cross section. Integrating the energy equation (9) across the pipe there is obtained

$$\frac{2\pi}{a^2} \int_0^a \overline{ruv} \frac{dU}{dr} dr = \frac{2\pi}{a^2} \int_0^a \overline{Wr} dr \tag{12}$$

which states that the total energy produced at a given section is dissipated at the same section because of the homogeneity of the field in the x-direction. Equation (12) was found to be satisfied within 10 per cent. It is remarked that if the isotropic relation between all terms had been assumed and the dissipation calculated in the usual way using

$$W = 15\nu \overline{\left(\frac{\partial u}{\partial x}\right)^2}$$

the right-hand side of equation (12) would have been smaller by approximately a factor of 2.5. It is still an open question, however, how accurate the approximation is from point to point.

#### Energy-Spectrum Measurements

The amplified hot-wire signal was fed into a Hewlett-Packard wave analyzer with a frequency range of 10 to 16,000 cycles per second. The analyzer selectivity characteristics were obtained by calibration; two fixed band widths were chosen, their effective values being 11 and 42 cycles per second approximately. The output of the analyzer was fed into a thermocouple circuit. In order to make the measurements independent of the amplifier frequency response the thermocouple output readings of the hot-wire signal were matched by a known sine-wave input.

The measurements are presented in figures 14, 15, and 16. Wire-length corrections were applied only to the  $u'$ -spectra, using the method described in reference 16.

#### DISCUSSION

As already pointed out in the "Introduction," the present understanding of the turbulence phenomenon is not complete enough to be able to attack directly the problem concerning the nature of the turbulence transfer mechanism that establishes a stable, nondecaying turbulence field such as the pipe flow. The principal aim of the present work was an attempt to obtain an over-all picture of the turbulence structure without trying to understand the detailed mechanism responsible for this structure. To this end the energy equations of both the mean and turbulent flow serve as a useful guide. The former in effect expresses the relative magnitude of the mean-flow energy loss to the turbulent field as compared with losses due to dissipation by direct molecular action. The latter gives a relation between the different forms of

turbulent-energy rates such as rates of production, dissipation, and diffusion. Unfortunately it is not possible to obtain from these equations any explicit information on how these various energy changes take place. However, it is hoped that once their relative importance in different regions of the turbulent field is better understood one might attack the ultimate problem of the turbulence mechanism with greater confidence.

A different, but already well-established, method of approach was also tried. Instead of investigating the different rates of changes of the turbulent energy at a given point of the field, its spectral distribution in the wave-number space was examined. The merits and shortcomings of this method will be discussed later.

#### Mean-Energy Balance

Multiplying the integrated momentum equation (6a) by the mean-velocity gradient  $dU/dr$ , the energy equation of the mean flow is obtained:

$$\frac{r}{a} U_{\tau}^2 \frac{dU}{dr} = \overline{uv} \frac{dU}{dr} - \nu \left( \frac{dU}{dr} \right)^2$$

Thus the energy available because of the pressure drop along the pipe is partly converted into turbulent energy and is partly directly dissipated. The two terms on the right-hand side of the equation are compared in a nondimensional form near the wall in figure 17. There are two points that should be noted here: (a) The bulk of the direct viscous dissipation takes place in a very narrow region,  $r^* < 15$ ; (b) the position where the laminar shearing stress is equal to the turbulent shearing stress (viscous dissipation equal to turbulence production) is found to be approximately at the same point where the maximum amount of energy is produced ( $r^* = 11.5$ ). This point is usually referred to as the edge of the laminar sublayer. It is seen that not only is the bulk of the energy taken from the mean flow directly dissipated but a considerable portion of the total turbulence production (20 percent) also takes place here.

It is quite apparent from this picture that, in order to obtain the complete picture of the turbulent-energy balance, conditions near and within the laminar sublayer have to be known. This, of course, is a very difficult task from the experimental point of view.

### Turbulent-Energy Balance

From the measurements presented in the previous section all the terms of the turbulent-energy equation (eq. (9)) can be calculated with the exception of the pressure-energy diffusion. Unfortunately, since this term is small everywhere except near the wall, its determination from equation (9) is very inaccurate. Nevertheless, it is possible to obtain in a qualitative way an over-all picture of the complete turbulent-energy balance at a cross section. Since the experimental problems and errors are different in the two Reynolds number flows they will be discussed separately.

Low Reynolds number flow.- In order to be able to study the flow conditions very close to the wall it is necessary to produce as thick a viscous layer as possible. This may be done by carrying out the measurements at very low mean speeds. Certain compromises, however, have to be made. First it is much more difficult to establish good flow conditions at low speeds, and second it is more difficult to carry out time-averaging processes in the measurements of statistical quantities. On the other hand the absolute magnitude of the dissipation terms may be better established since problems such as wire-length effects, amplifier frequency response, and noise are not so critical.

Figures 18 and 19 give the distribution of all the energy terms in the low Reynolds number flow. It should be noted that in forming dimensionless quantities for the coordinates, the characteristic length  $a$  was chosen in figure 18 and  $v/U_\tau$  was used in figure 19 representing conditions near the wall. The correspondence between respective coordinates is indicated parenthetically in figure 19.

The following interesting conclusions may be drawn:

(1) Throughout the whole cross section, with the exception of the center region, the rate of energy production at a point is approximately balanced by the rate of energy dissipation.

(2) All the various energy rates reach a sharp maximum near the edge of the laminar sublayer.

(3) This edge appears to be also the region from which the turbulent kinetic energy is diffusing both toward the pipe center and toward the wall and toward which the pressure energy is transported.

There is some question about the direction of the pressure diffusion in the center region of the pipe. It was mentioned in the previous section that the measured triple velocity correlations are believed to be too low in this region. Assuming that their dimensionless value is

approximately the same as the values found in the high Reynolds number flow - an assumption which holds approximately true for all other measured dimensionless statistical quantities - kinetic-energy diffusion is estimated as shown with a dashed line in figure 18. It is believed that the corresponding pressure-diffusion distribution (dashed line) comes closer to the actual picture than that obtained from the directly measured points (solid line). This would indicate that the direction of the pressure diffusion is toward the laminar sublayer and its value near the center is close to zero.

High Reynolds number flow.- As already pointed out, accurate measurements of the various dissipation terms in the case of high Reynolds number flow become much more difficult, since, because of the extent of the energy spectrum to high frequencies, amplifier-tube noise and wire-length effects become increasingly more critical. Although all precautions were made to minimize these effects, the calculated rate of energy dissipation is believed to be too small. From the energy-spectrum measurements it was possible to infer that considerable dissipation takes place at frequencies as high as 30,000 cycles per second where the response of the compensated amplifier ceases to be linear. From the information gathered in the low Reynolds number flow, an attempt was made to estimate the dissipation. The following assumptions were made: (1) In the vicinity of the wall where similarity with respect to Reynolds number was found (this will be discussed in detail later) the dissipation can be obtained directly from the low Reynolds number measurements; (2) the errors in percentage are the same across the pipe. This was found to be fairly closely true when the dissipation measurements were repeated using various high-frequency cut-off filters. With these assumptions and with equation (12) the estimated dissipation was obtained. Figures 20 and 21 show the directly measured and estimated values. The figures also indicate that the picture of the energy balance is similar to that obtained in the low Reynolds number flow.

#### Energy-Spectrum Considerations

In the study of isotropic turbulence the concept of the energy spectrum proved to be a useful and a convenient one both from an analytical and a physical point of view. By considering the distribution of the turbulent energy in the wave-number space it is possible to give in many instances a simple picture of some basic physical processes taking place in the field. An example is the commonly accepted picture of the energy transfer from smaller to larger wave numbers.

The utility of the spectrum function is much more restricted in a nonisotropic turbulence field where it cannot be contracted into a scalar, as in the isotropic case, but has to be treated as a tensor quantity. A restrictive factor in all cases, and particularly in nonisotropic turbulence, is the fact that measurement is possible of only the so-called

Taylor, or time, spectrum. This means that, even if Taylor's hypothesis (eq. (11)) is fulfilled, only a spatial energy distribution over a surface  $k_1 = \text{Constant}$  can be measured. This, of course, prohibits detailed knowledge of the point-by-point energy distribution in the wave-number space. Nevertheless, it is possible to draw some conclusions from this type of measurements.

The measured  $u'$ -spectra (fig. 14) indicate that the spectral distributions obtained not too close to the wall manifest similar behavior over a wide range of wave numbers. Specifically, they vary as the  $-5/3$  power of the wave number  $k_1$  over a considerable range. This is clearly indicated in figure 22 where the function  $k_1^{5/3} F_u(k_1)$  is shown to be a constant over the range  $1 < k_1 < 24$ . The two sets of points shown in this figure indicate the magnitude of the length corrections applied to the directly measured values. This, of course, is the same type of behavior as that of the equilibrium range of the energy spectrum in an isotropic field first predicted by Kolmogoroff (ref. 17). One may infer therefore that for sufficiently large turbulent Reynolds number flows ( $u'\lambda/\nu > 200$  for all measurements) and for the mean-velocity gradients not too large there exists a wide range of wave numbers in which the energy represented by the  $u'$ -component is transferred from smaller to larger wave numbers without being significantly influenced by the turbulent-energy production mechanism or by viscous dissipation. This apparently is true, even though local isotropy does not exist in this range as will be seen later. It is further seen that this range varies with  $r'/a$  and at  $r'/a = 0.0082$ , where the mean-velocity gradient is already large, the spectrum shows a different distribution. It might be mentioned that in this case there is a rather wide wave-number range where the spectrum varies closely as  $k_1^{-1}$  as predicted by Tchen (ref. 3).

The conclusions one may draw from the measurements of the  $v'$ - and  $w'$ -spectra are significantly different. In order to clarify this difference a comparison is made between the  $v'$ -spectrum measured at the center of the pipe and that calculated from the measured  $u'$ -spectrum using isotropic relations (fig. 23). It is seen that there is a large energy deficiency in the low wave-number range, while the energy content of the higher wave numbers is much larger. Furthermore, the  $-5/3$ -power-law type of distribution is completely missing. Similar statements may be made for the  $v'$ -spectra (and  $w'$ -spectra) at points other than the center of the pipe. An explanation of such behavior is, of course, difficult mainly because the one-dimensional nature of the measurements conceals the detailed spatial energy distribution. However, it is hard to conceive that the geometry of the field alone would be responsible for such a behavior. Figure 23 may suggest that wave numbers receive a large portion of their  $v'$  energy not only by means of the usual transfer mechanism from smaller to larger wave numbers. By considering

the energy equations for the turbulent components separately, the term most likely to influence the  $v'$ -spectrum in the wave-number range considered is the pressure term transferring energy from one velocity component to the other. Its form  $p \frac{\partial v}{\partial r}$  suggests that it is associated

with wave numbers larger than those where the bulk of the turbulent energy is produced and smaller than the ones where viscous dissipation is important. This term therefore may very well be responsible for the larger  $v'$  energy present in the wave-number range in question. It is difficult to draw any conclusion about the role played by the diffusion terms; in general they are thought of as representing a low-frequency phenomenon and therefore would influence the  $v'$ -spectrum in the low wave-number range only.

It should be emphasized that the above discussion is merely speculative in nature and a considerable amount of experimental work especially in connection with the pressure terms is necessary to be able to give a quantitative picture of the energy balance spectrumwise.

#### General Considerations

On the basis of the presented measurements the flow field in the pipe may be divided into three regions exhibiting different behavior from the point of view of turbulence structure.

Wall-proximity range.- Measurements near the wall indicate that the well-known wall-proximity law of Prandtl (ref. 18) for the mean velocity may be extended to the fluctuating-velocity field also. Thus by using  $U_T$  and  $v/U_T$  as the characteristic velocity and length parameters, the various velocity distributions become independent of the Reynolds number in the approximate range  $0 < r^* < 30$  (figs. 24 to 26).

The various energy rates as they appear in the equation of turbulent energy are found to be of equal relative importance; their magnitudes are much larger than those in other regions of the turbulent field and they therefore play a dominant role in the energy balance over the entire field.

Center portion of pipe.- Since the direct effect of viscosity on the turbulent field is negligible in the center portion of the pipe, it may be expected that the distributions of the fluctuations expressed relative to the characteristic velocity  $U_T$  are independent of the Reynolds number. Figures 5, 7, and 8 show this to be the case.

This region is further characterized by the fact that it receives a large portion of its turbulent energy by diffusive action.

Intermediate region.- The intermediate range extends from  $r^* \approx 100$  to  $r'/a \approx 0.1$ . By considering the turbulent-energy balance in this region (fig. 21) it is seen that the rate of energy diffusion is much smaller than that of production or dissipation. This means that the energy produced here is locally dissipated. It should be noted that this is one of the implied assumptions of the mixing-length theories. Another assumption, namely the existence of statistical similarity between the velocity components, is, however, difficult to accept in view of the discussion in the section "Energy-Spectrum Considerations." Thus, although the gradient type of momentum transfer involved in mixing-length theories has more experimental support in this region than in other portions of the field, its use is not completely justifiable.

#### SUMMARY OF RESULTS

Fully developed flow in a large pipe was found to provide a very useful medium in which to study the structure of turbulence in shear flow. Embodied in the term "structure" are the interactions between turbulent motions and mean flow, and the various transfers and movements of energy from point to point and from mean flow through the spectrum of turbulent motions.

The following are the major results:

1. The importance of a detailed knowledge of conditions in the close proximity of the wall was demonstrated.
2. Using the similarity parameters  $U_\tau$  and  $v/U_\tau$  the flow field in this region was shown to be independent of the Reynolds number.
3. The various turbulent-energy rates, such as production, diffusion, and dissipation, were found to reach a sharp maximum at the edge of the laminar sublayer ( $r^* \approx 12$ ), their magnitude being of equal relative importance but much larger than those in other regions of the pipe cross section.
4. It was found that there exist a strong transfer of kinetic energy away from the edge of the laminar sublayer and an equally strong movement of pressure energy toward it.
5. In the center region of the pipe, the characteristic length and velocity parameters were shown to be  $a$  and  $U_\tau$ .
6. In the region of large mean-velocity gradients but outside of the dissipative region (between  $r^* \approx 100$  and  $r'/a \approx 0.1$ ) energy diffusion was found to be small compared with the turbulent-energy production.

7. The spectrum measurements indicated that in regions where the mean-velocity gradients are not too large the  $u'$ -spectra vary as the  $-5/3$  power of the wave number over a considerable wave-number range.

8. A considerably different distribution of the  $v'$ - and  $w'$ -spectra was measured and an explanation of such a behavior was attempted.

National Bureau of Standards,  
Washington, D. C., October 28, 1952.

## REFERENCES

1. Batchelor, G. K.: Note on Free Turbulent Flows, with Special Reference to the Two-Dimensional Wake. Jour. Aero. Sci., vol. 17, no. 7, July 1950, pp. 441-445.
2. Rotta, J.: Statistische Theorie nichthomogener Turbulenz.
  1. Mitteilung. Zs. Phys., Bd. 129, 1951, pp. 547-572;
  2. Mitteilung. Zs. Phys., Bd. 131, 1951, pp. 51-77.
3. Tchen, C. M.: On the Spectrum of Energy in Turbulent Shear Flow. Res. Paper RP 2388, Jour. Res., Nat. Bur. Standards, vol. 50, no. 1, Jan. 1953, pp. 51-62.
4. Corrsin, Stanley: Investigation of Flow in an Axially Symmetrical Heated Jet of Air. NACA WR W-94, 1943. (Formerly NACA ACR 3123.)
5. Townsend, A. A.: The Fully Developed Turbulent Wake of a Circular Cylinder. Australian Jour. Sci. Res., ser. A, vol. 2, no. 4, Dec. 1949, pp. 451-468.
6. Corrsin, Stanley, and Uberoi, Mahinder S.: Spectra and Diffusion in a Round Turbulent Jet. NACA Rep. 1040, 1951. (Supersedes NACA TN 2124.)
7. Liepmann, Hans Wolfgang, and Laufer, John: Investigations of Free Turbulent Mixing. NACA TN 1257, 1947.
8. Townsend, A. A.: The Structure of the Turbulent Boundary Layer. Proc. Cambridge Phil. Soc., vol. 47, pt. 2, Apr. 1951, pp. 375-395.
9. Laufer, John: Investigation of Turbulent Flow in a Two-Dimensional Channel. NACA Rep. 1053, 1951. (Supersedes NACA TN 2123.)
10. Kampé de Fériet, J.: Sur l'écoulement d'un fluide visqueux incompressible entre deux plaques parallèles indéfinies. La Houille blanche, vol. 3, no. 6, Nov.-Dec. 1948, pp. 509-517.
11. Von Kármán, Th.: The Fundamentals of the Statistical Theory of Turbulence. Jour. Aero. Sci., vol. 4, no. 4, Feb. 1937, pp. 131-138.
12. Kovásznay, Leslie S. G.: Development of Turbulence-Measuring Equipment. NACA TN 2839, 1953.
13. Townsend, A. A.: Measurement of Double and Triple Correlation Derivatives in Isotropic Turbulence. Proc. Cambridge Phil. Soc., vol. 43, pt. 4, Oct. 1947, pp. 560-570.

14. Lin, C. C.: On Taylor's Hypothesis and the Acceleration Terms in the Navier-Stokes Equations. NAVORD Rep. 2306, Naval Ord. Lab., Mar. 31, 1952.
15. Taylor, G. I.: Statistical Theory of Turbulence. III - Distribution of Dissipation of Energy in a Pipe Over Its Cross-Section. Proc. Roy. Soc. (London), ser. A, vol. 151, no. 873, Sept. 2, 1935, pp. 455-464.
16. Uberoi, Mahinder S., and Kovaszny, Leslie S. G.: On Mapping and Measurement of Random Fields. Quart. Appl. Math., vol. X, no. 4, Jan. 1953, pp. 375-393.
17. Kolmogoroff, A.: The Local Structure of Turbulence in Incompressible Viscous Fluid for Very Large Reynolds' Numbers. Comp. rend., acad. sci. URSS, vol. 30, no. 4, Feb. 10, 1941, pp. 301-305.
18. Prandtl, L.: Bericht über Untersuchungen zur ausgebildeten Turbulenz. Z.a.M.M., Bd. 5, Heft 2, Apr. 1925, pp. 136-139.

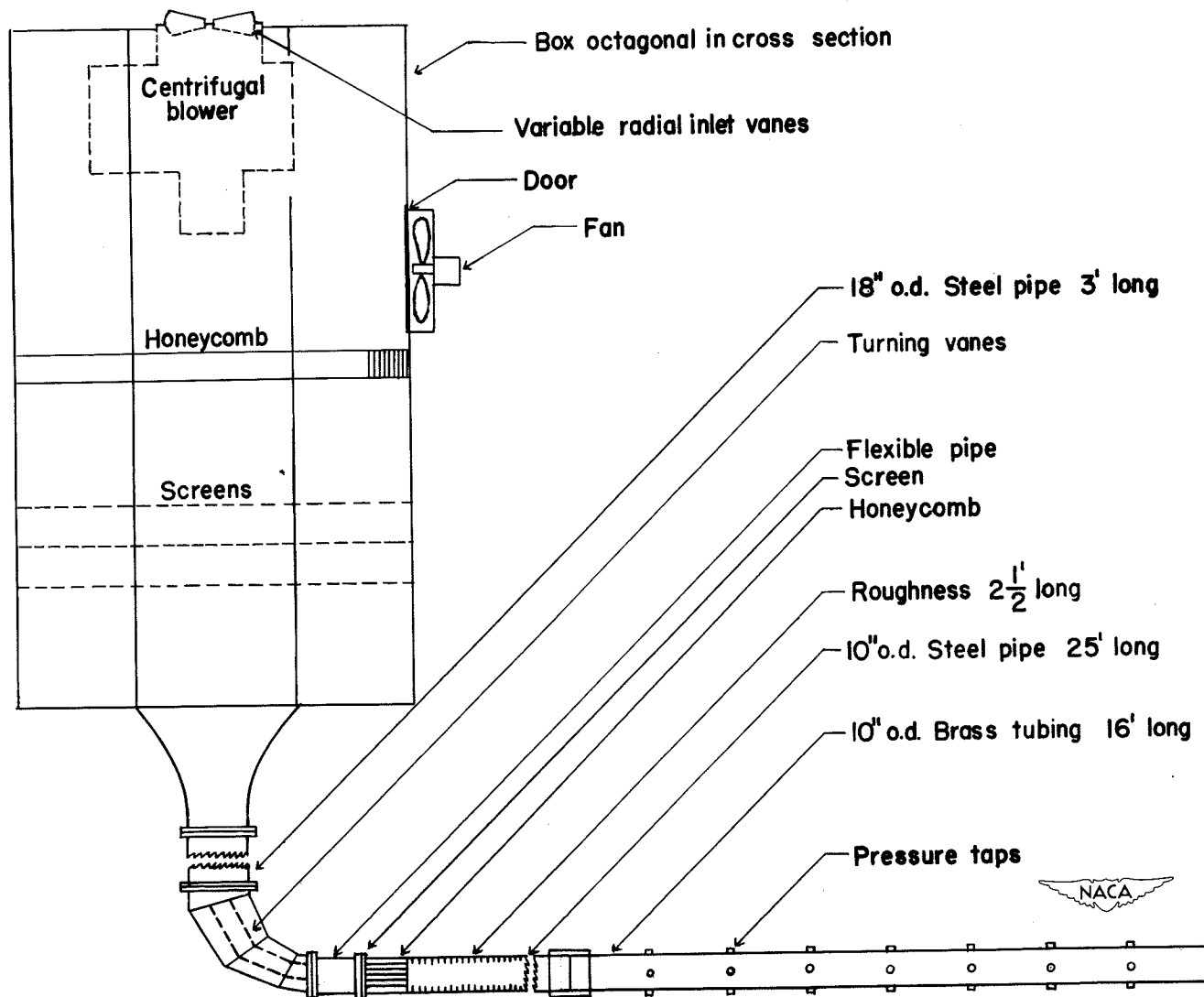


Figure 1.- Schematic diagram of test setup.

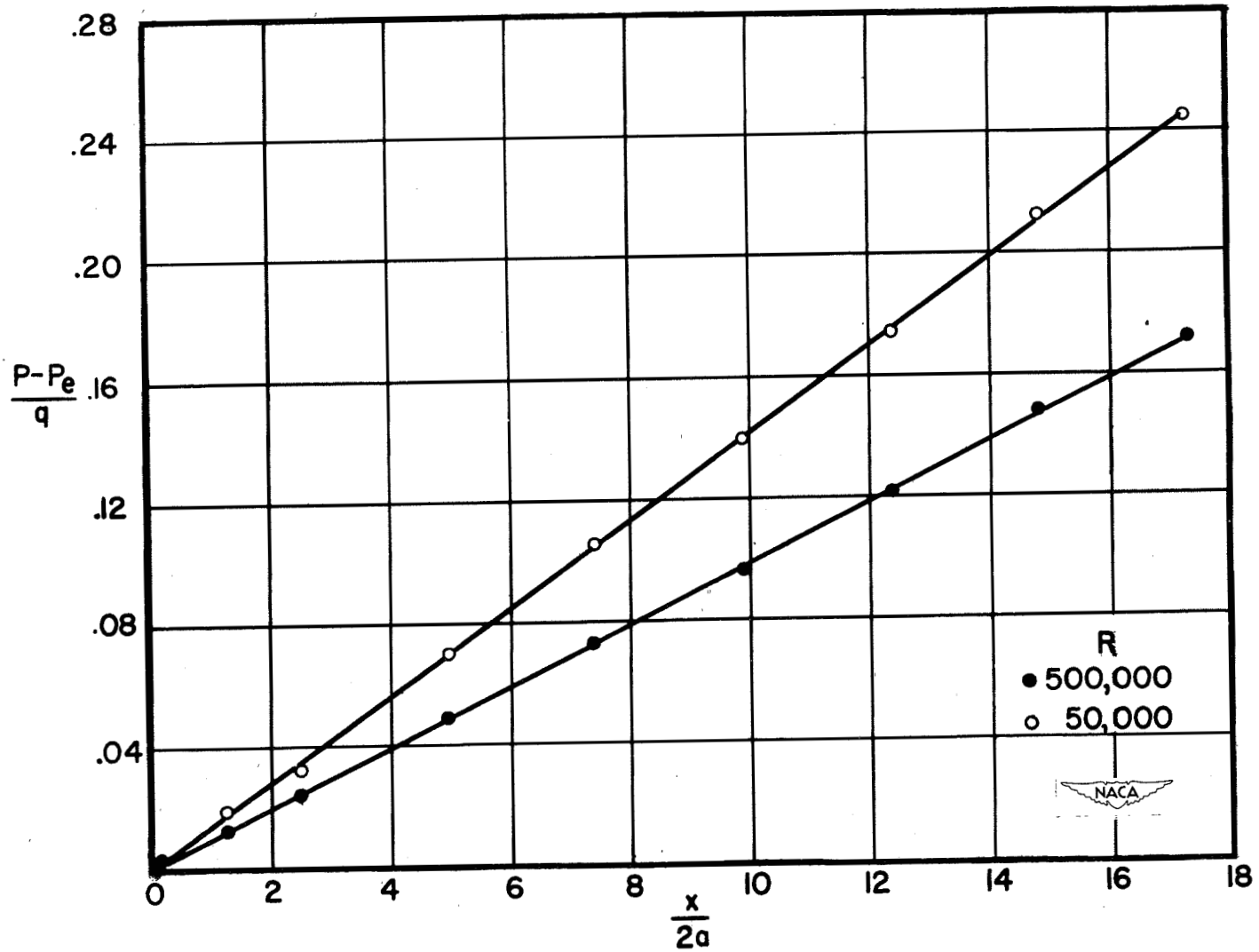


Figure 2.- Mean-pressure distribution along pipe axis.

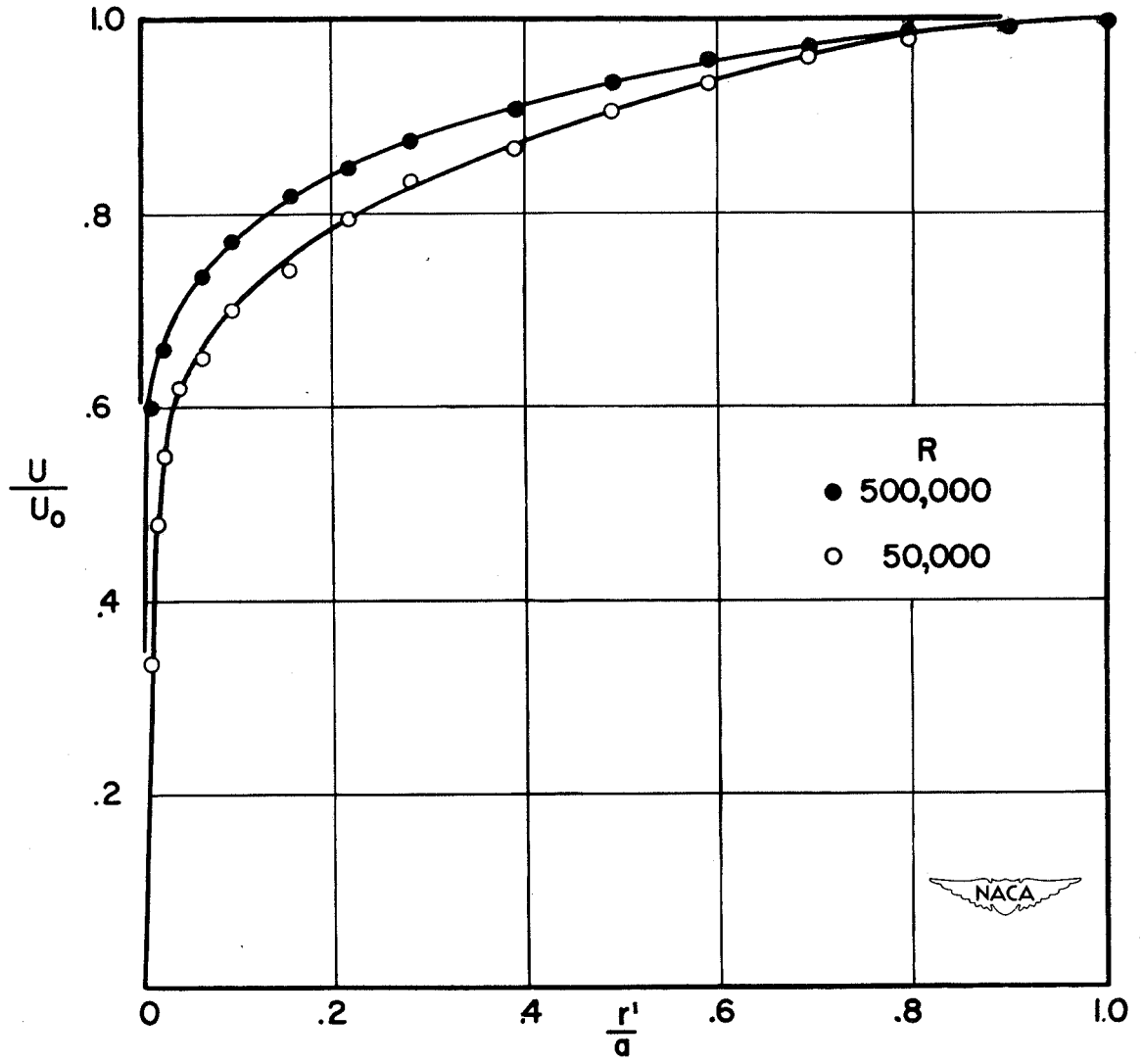


Figure 3.- Mean-velocity distribution.

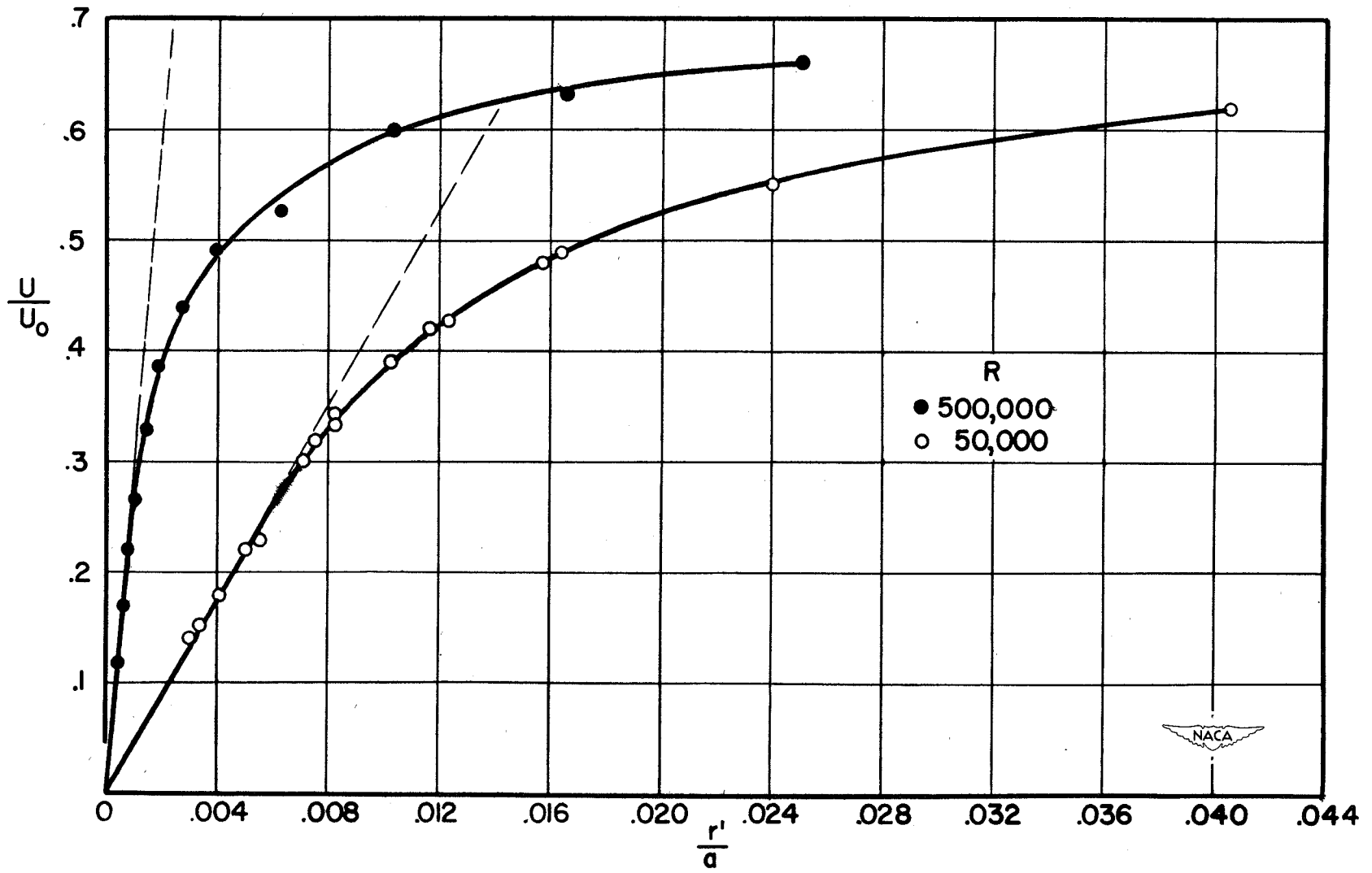


Figure 4.- Mean-velocity distribution near wall. Dashed lines are computed from pressure-drop measurements.

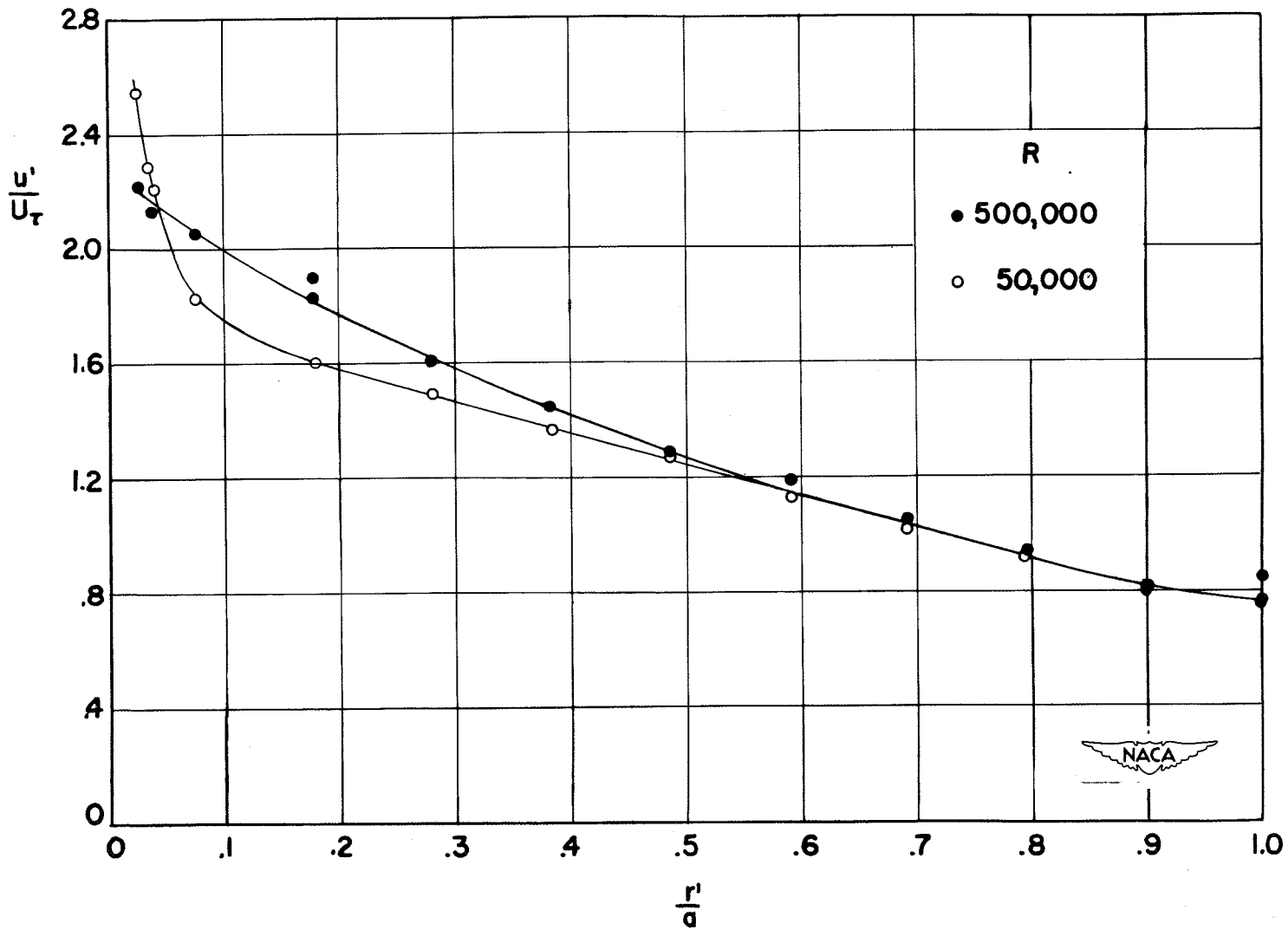


Figure 5.-  $u'$  distribution.

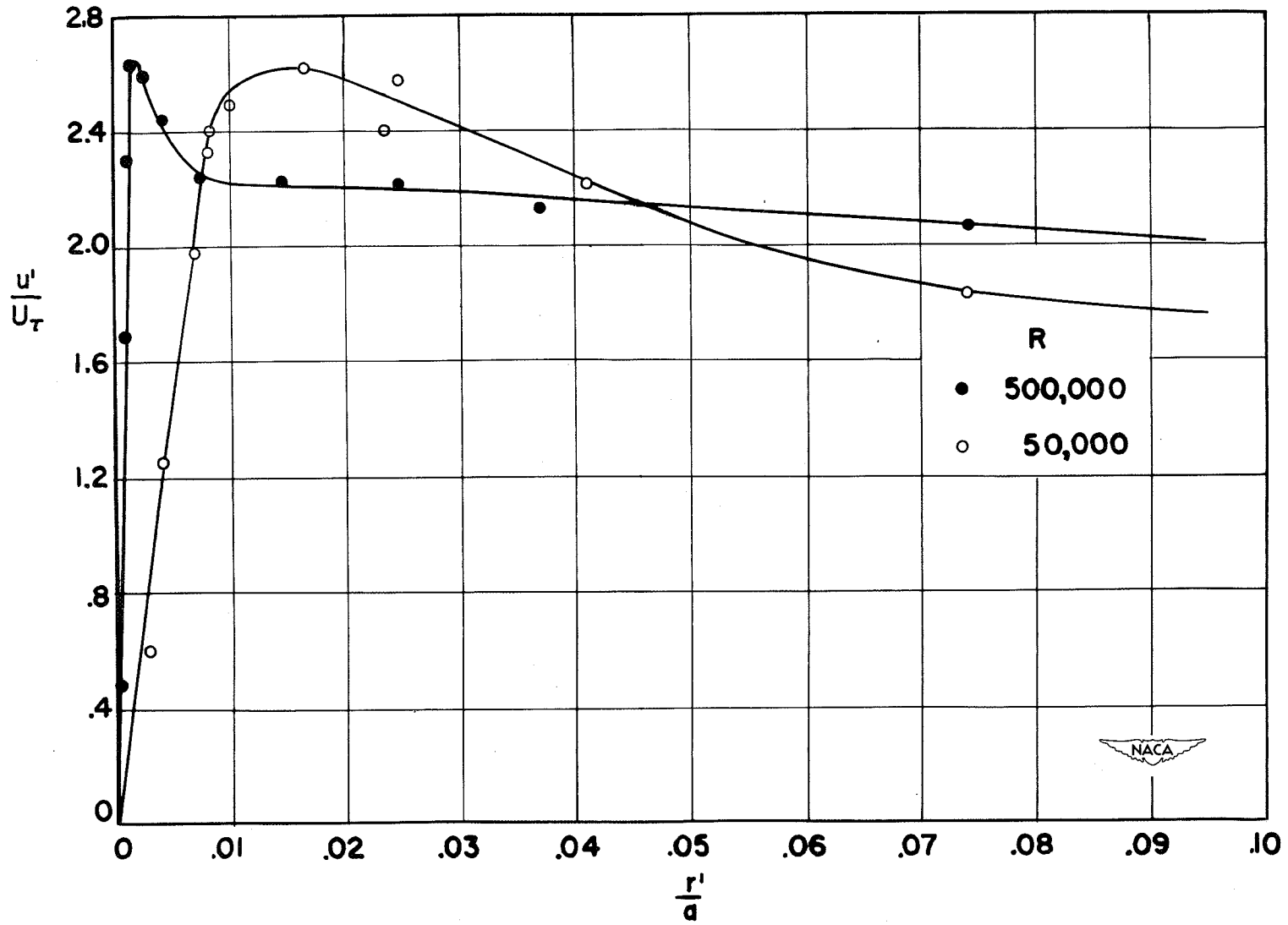


Figure 6.-  $u'$  distribution near wall.

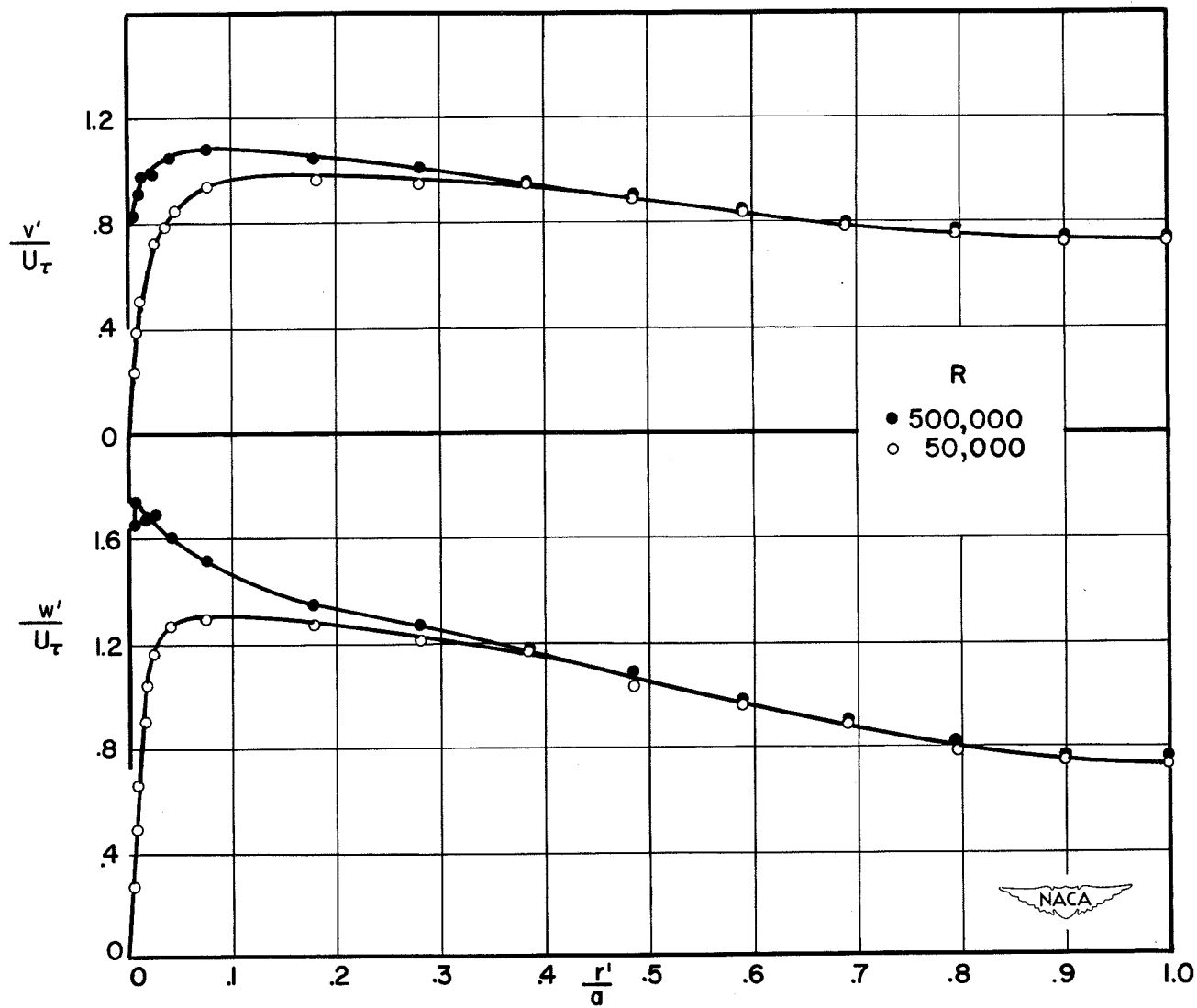


Figure 7.-  $v'$  and  $w'$  distributions.

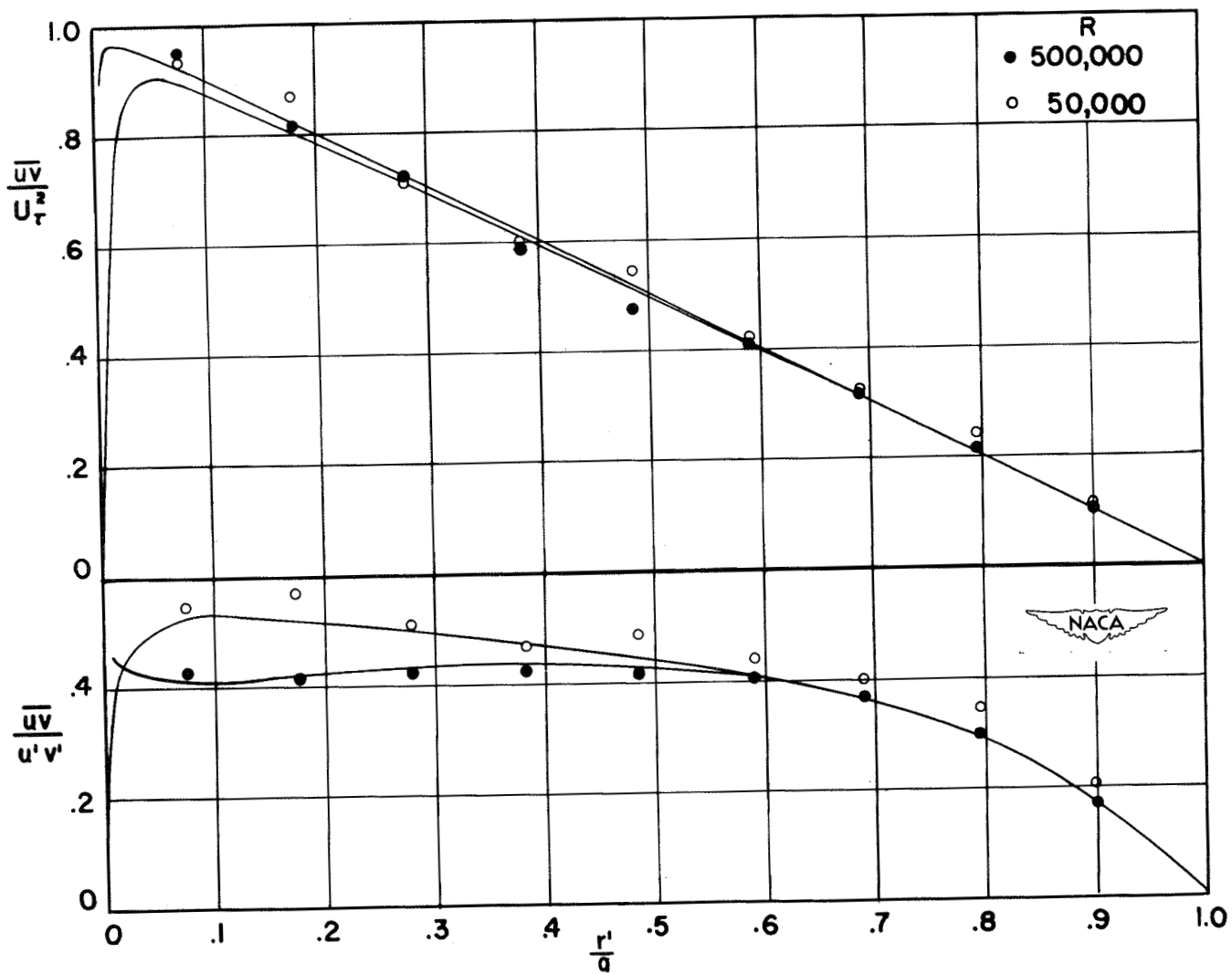


Figure 8.- Reynolds shearing stress and double-correlation-coefficient distributions. Curves calculated from measured  $dU/dr$ ,  $u'$ , and  $v'$ .

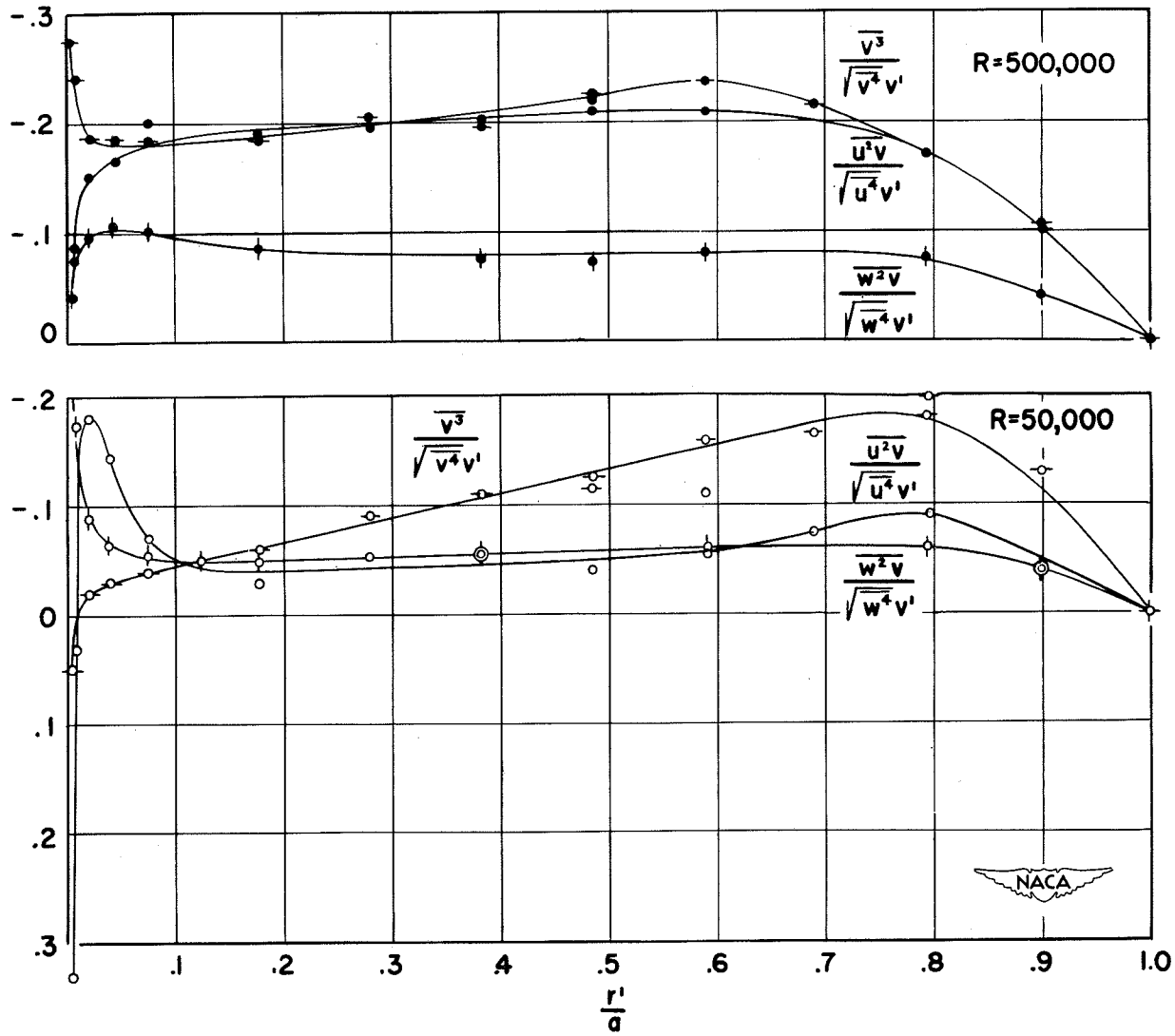


Figure 9.- Triple-correlation coefficients.

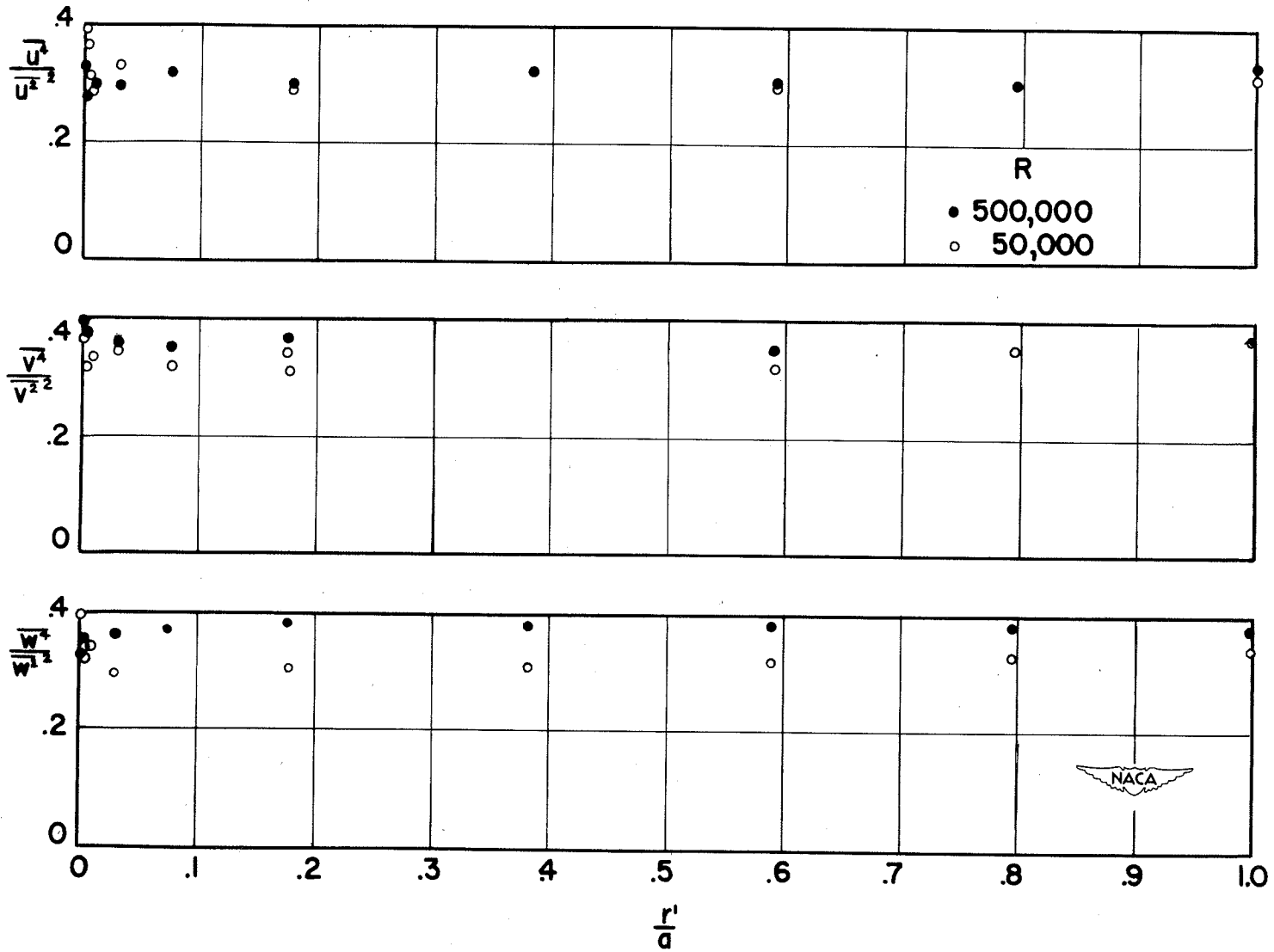


Figure 10.- Quadruple-correlation coefficients.

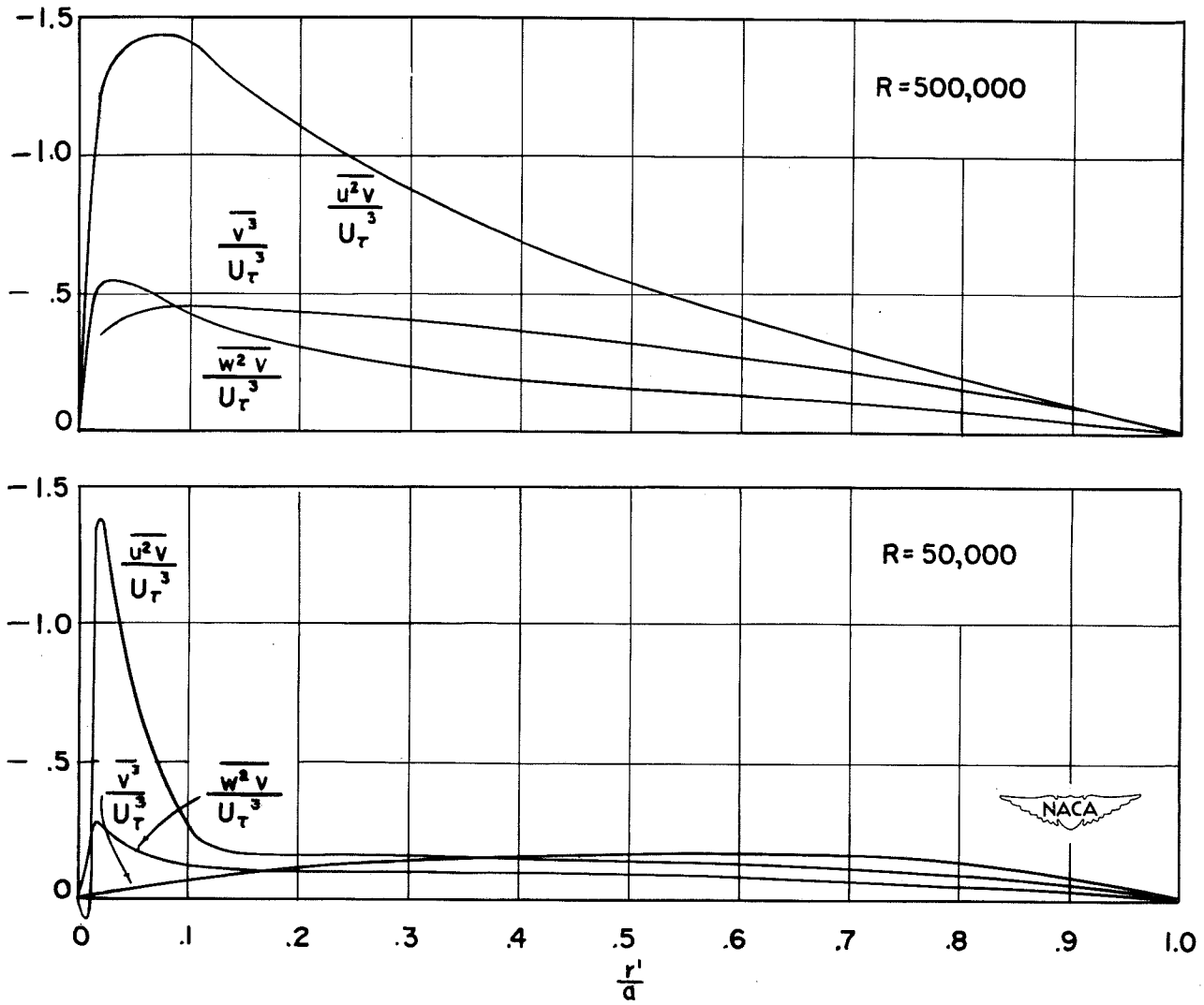


Figure 11.- Triple-velocity-correlation distributions.

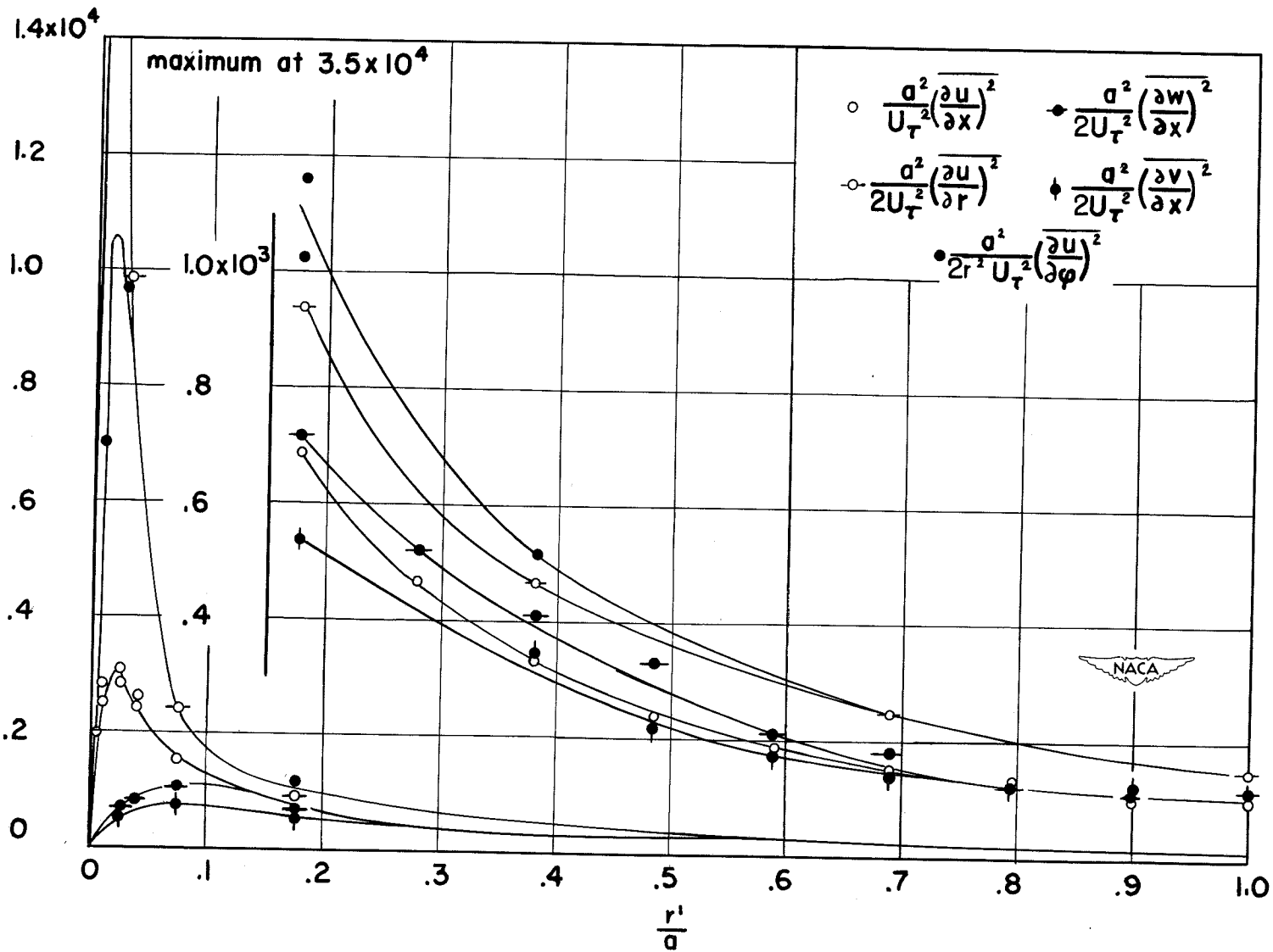


Figure 12.- Distributions of dissipation terms.  $R = 50,000$ .

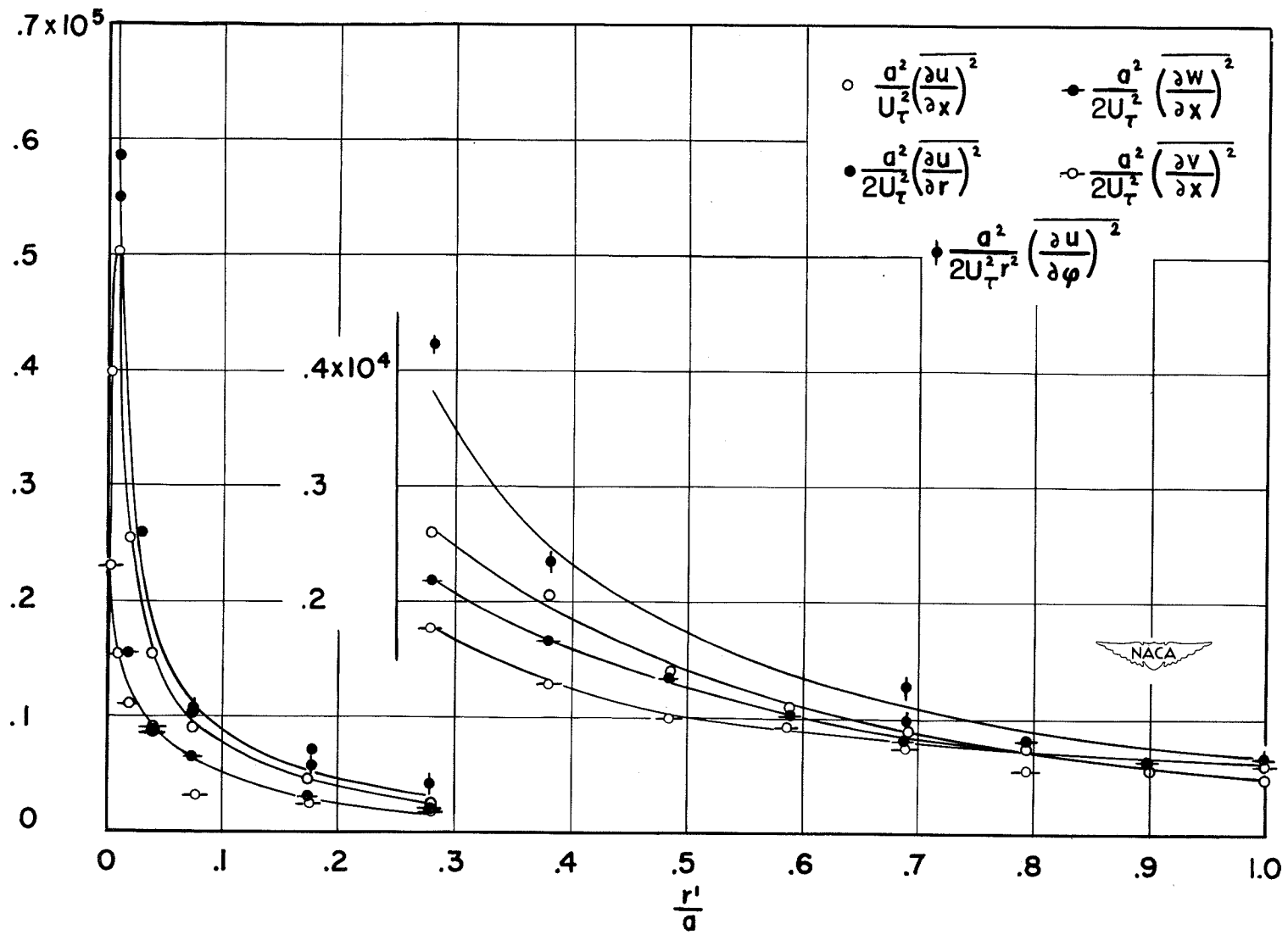


Figure 13.- Distributions of dissipation terms.  $R = 500,000$ .

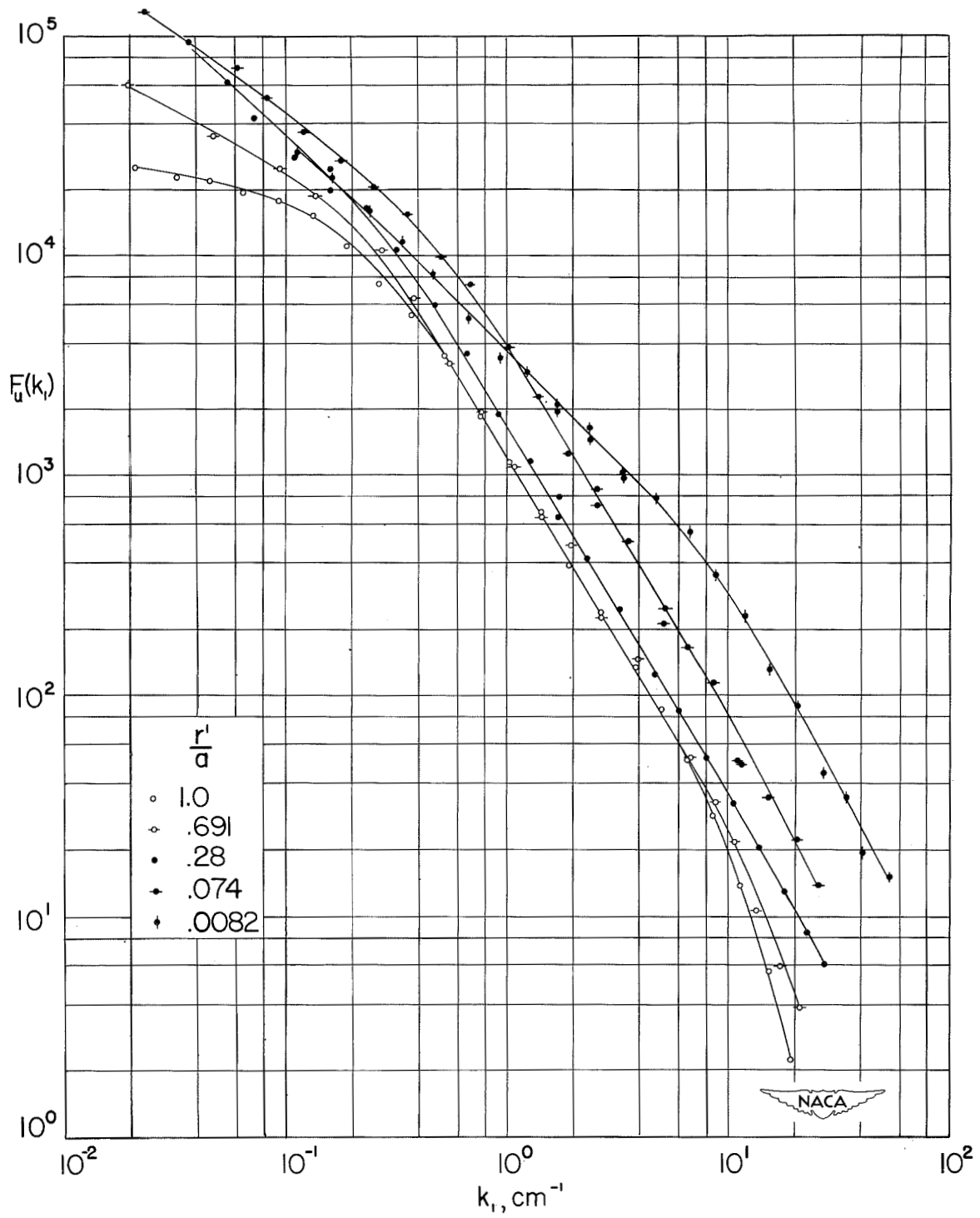
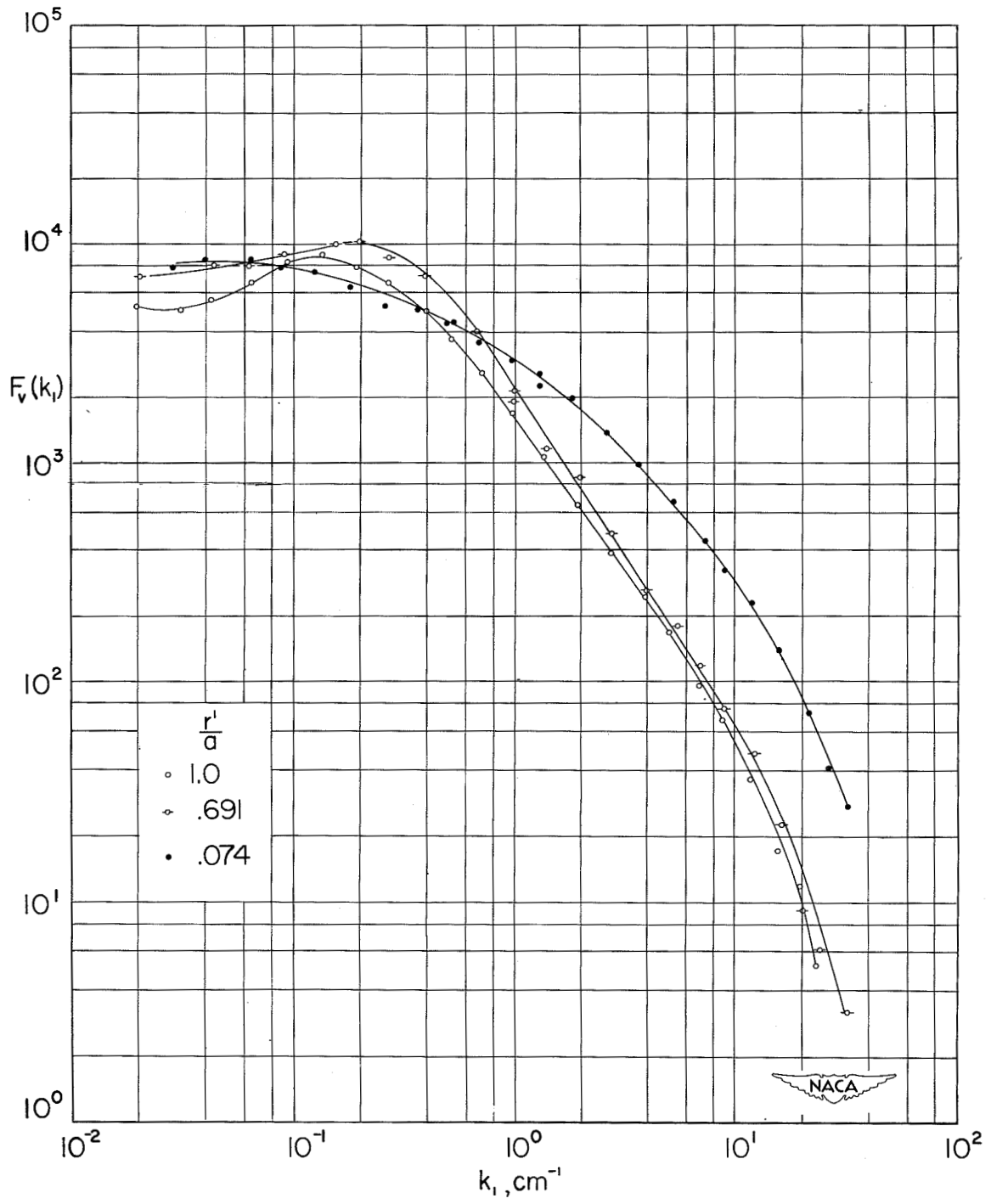


Figure 14.-  $u'$ -spectra.  $R = 500,000$ .

Figure 15.-  $v'$ -spectra.  $R = 500,000$ .

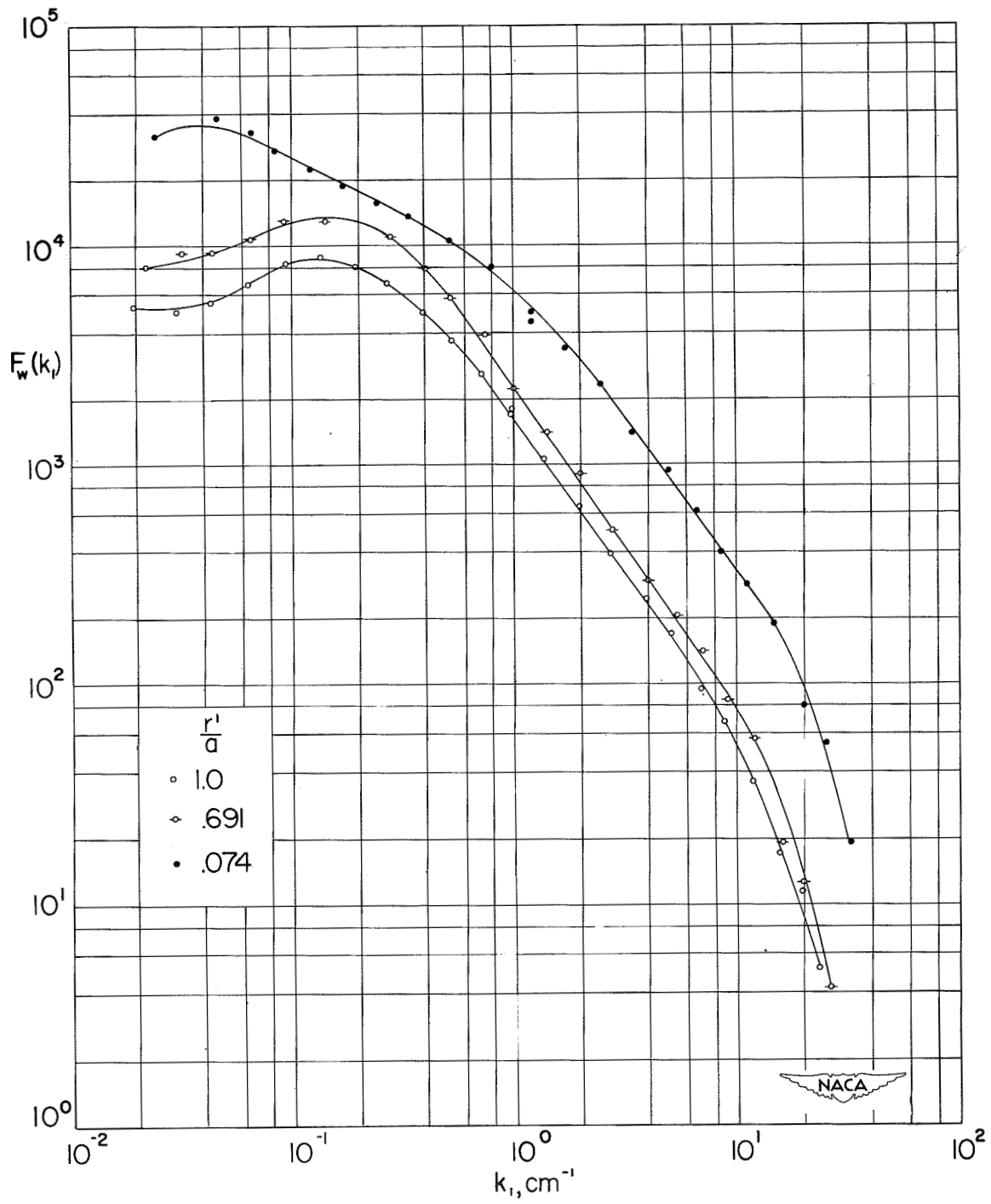


Figure 16.-  $w'$ -spectra.  $R = 500,000$ .

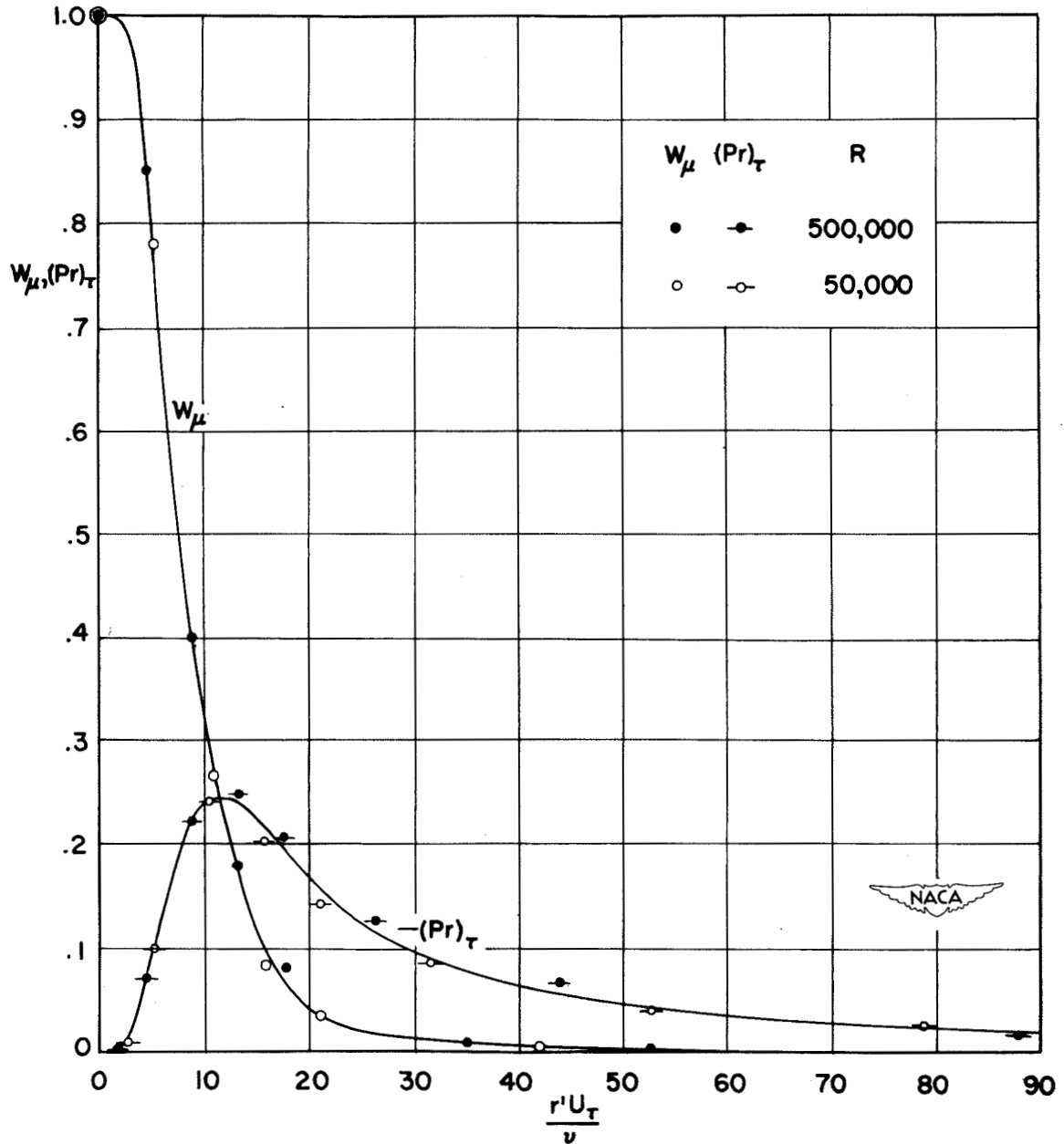


Figure 17.- Comparison of rate of turbulent-energy production with direct-viscous-dissipation rate near wall.

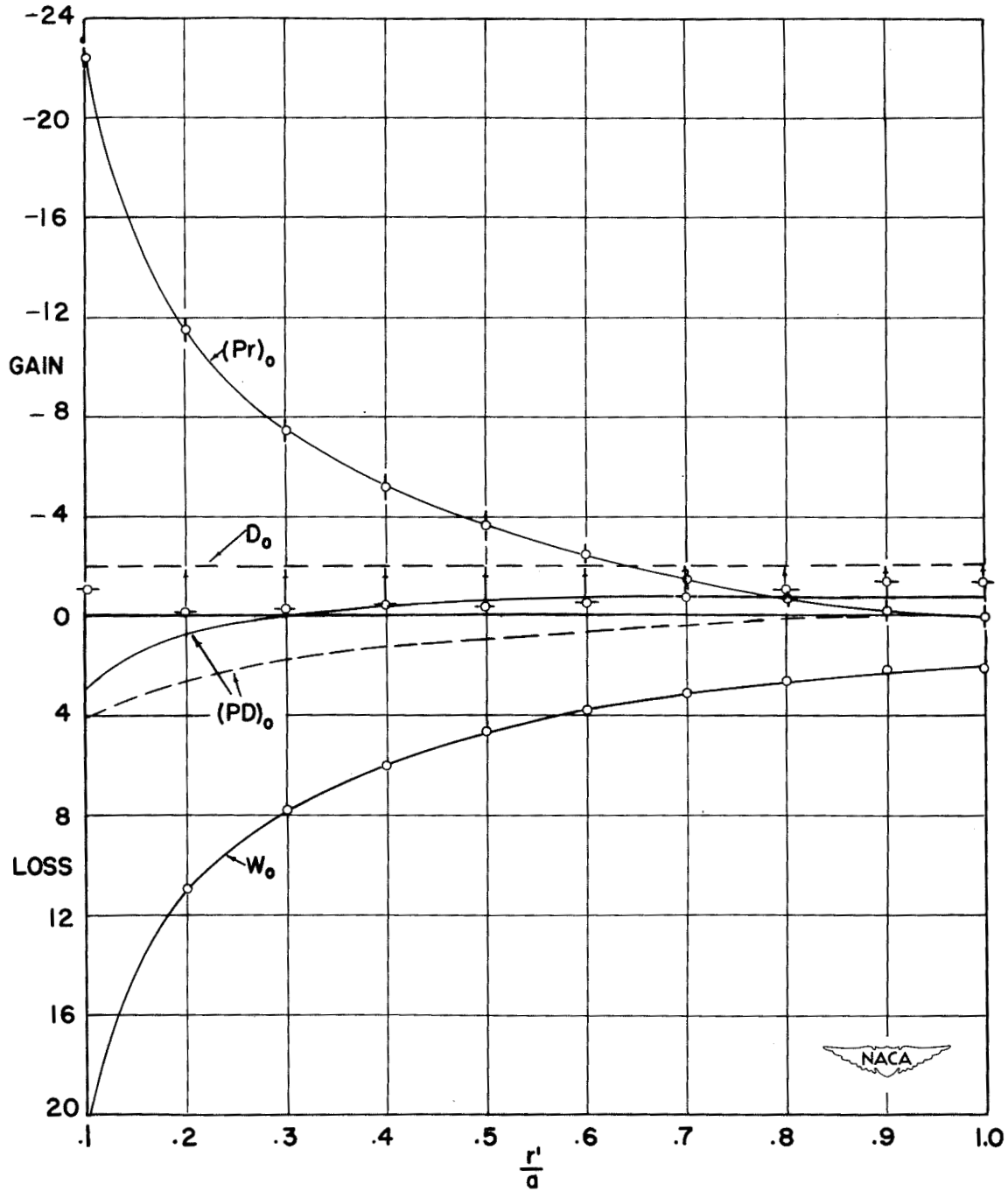


Figure 18.- Turbulent-energy balance.  $R = 50,000$ . Dashed lines are estimated.

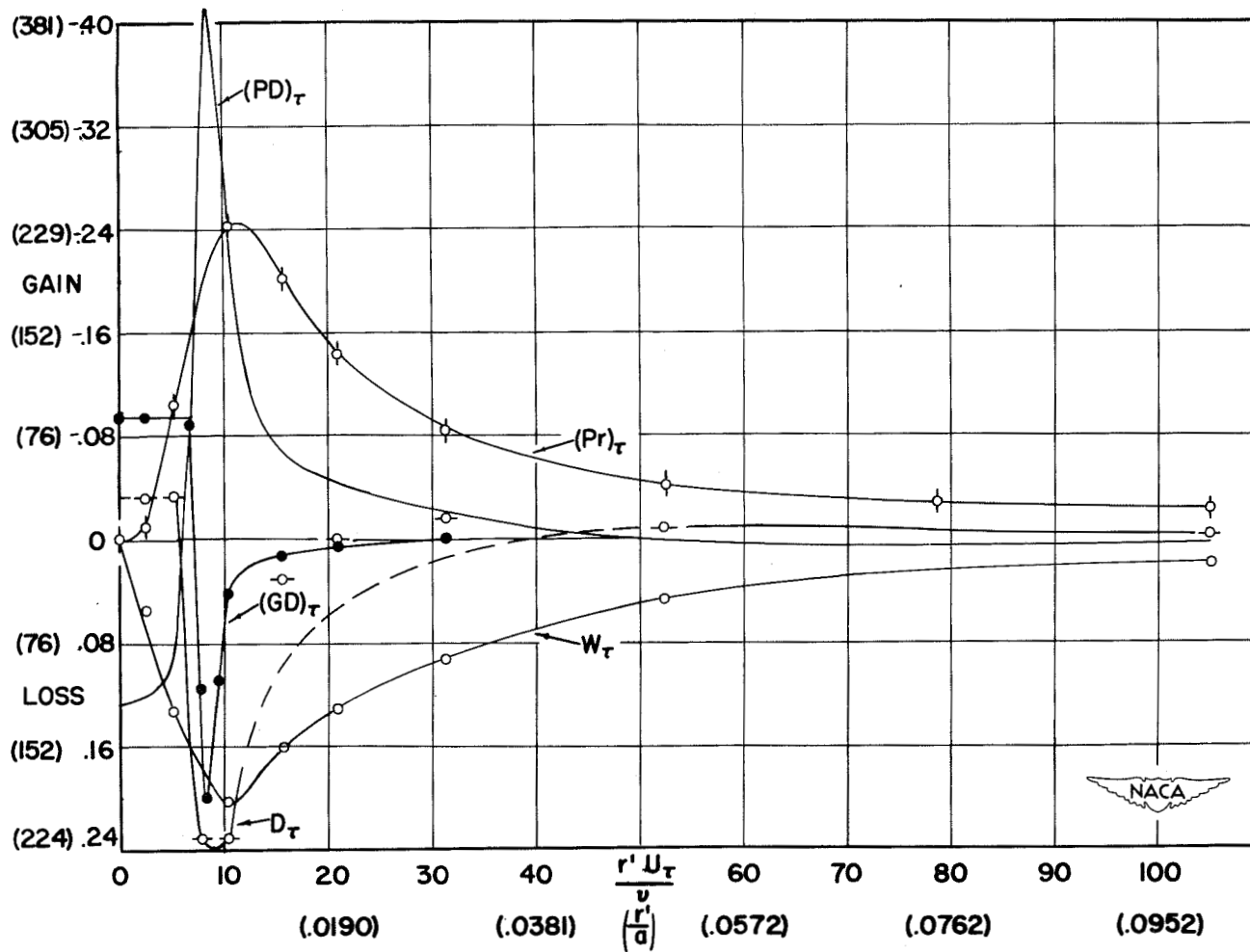


Figure 19.- Turbulent-energy balance near wall.  $R = 50,000$ . Numbers in parentheses along ordinate correspond to subscript  $\tau$ , as in figure 18. Dashed lines are estimated.

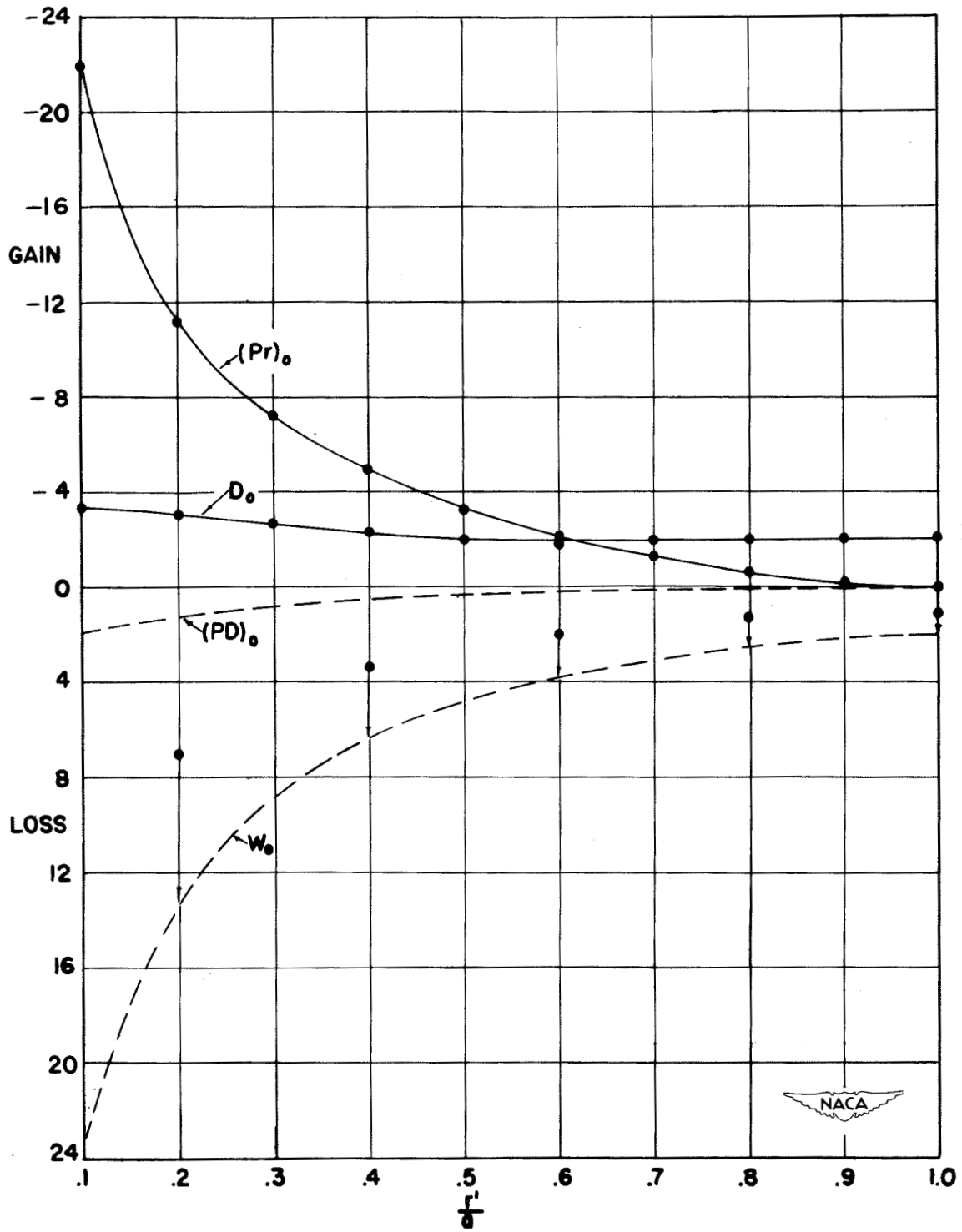


Figure 20.- Turbulent-energy balance.  $R = 500,000$ . Dashed lines are estimated.

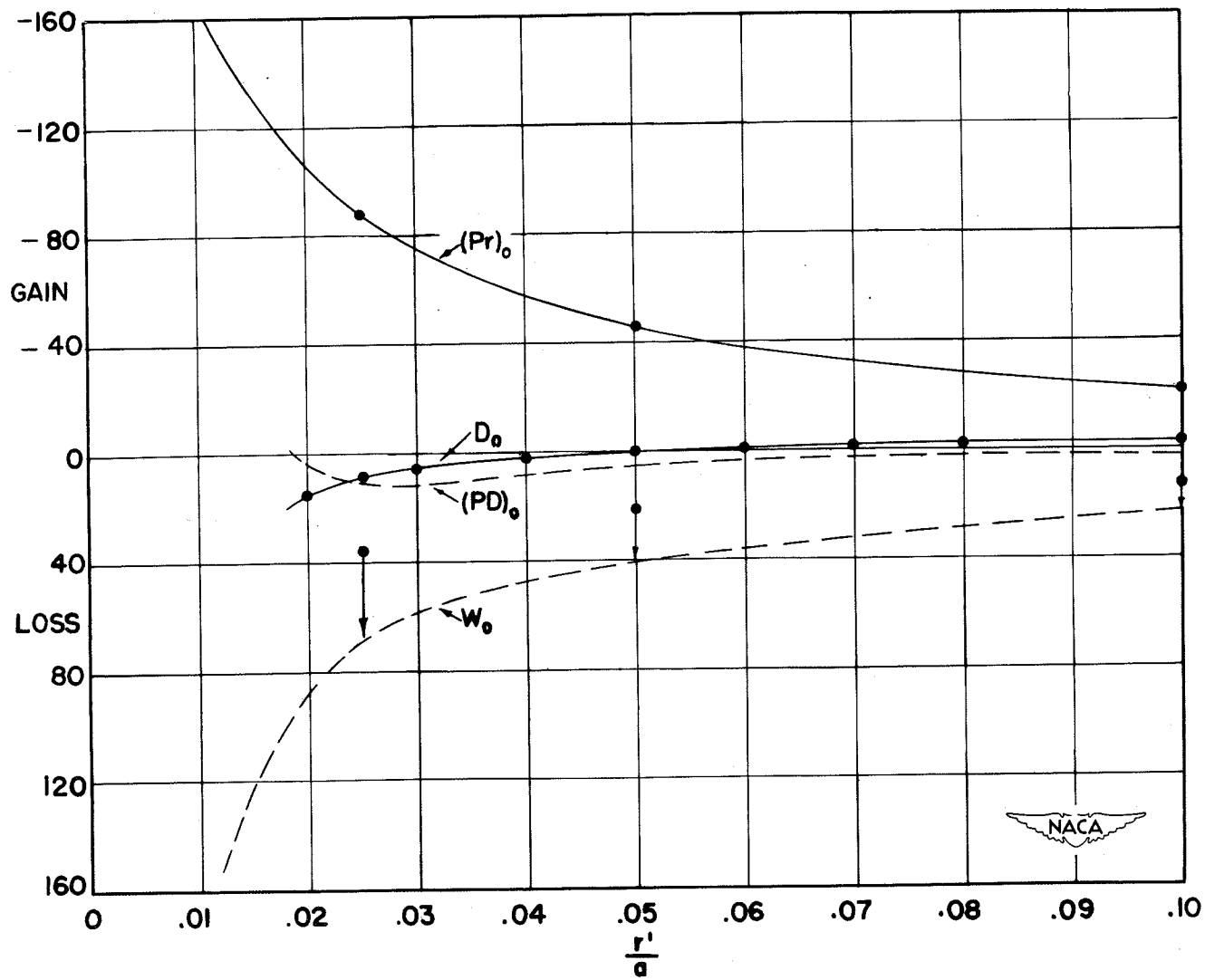


Figure 21.- Turbulent-energy balance near wall.  $R = 500,000$ . Dashed lines are estimated.

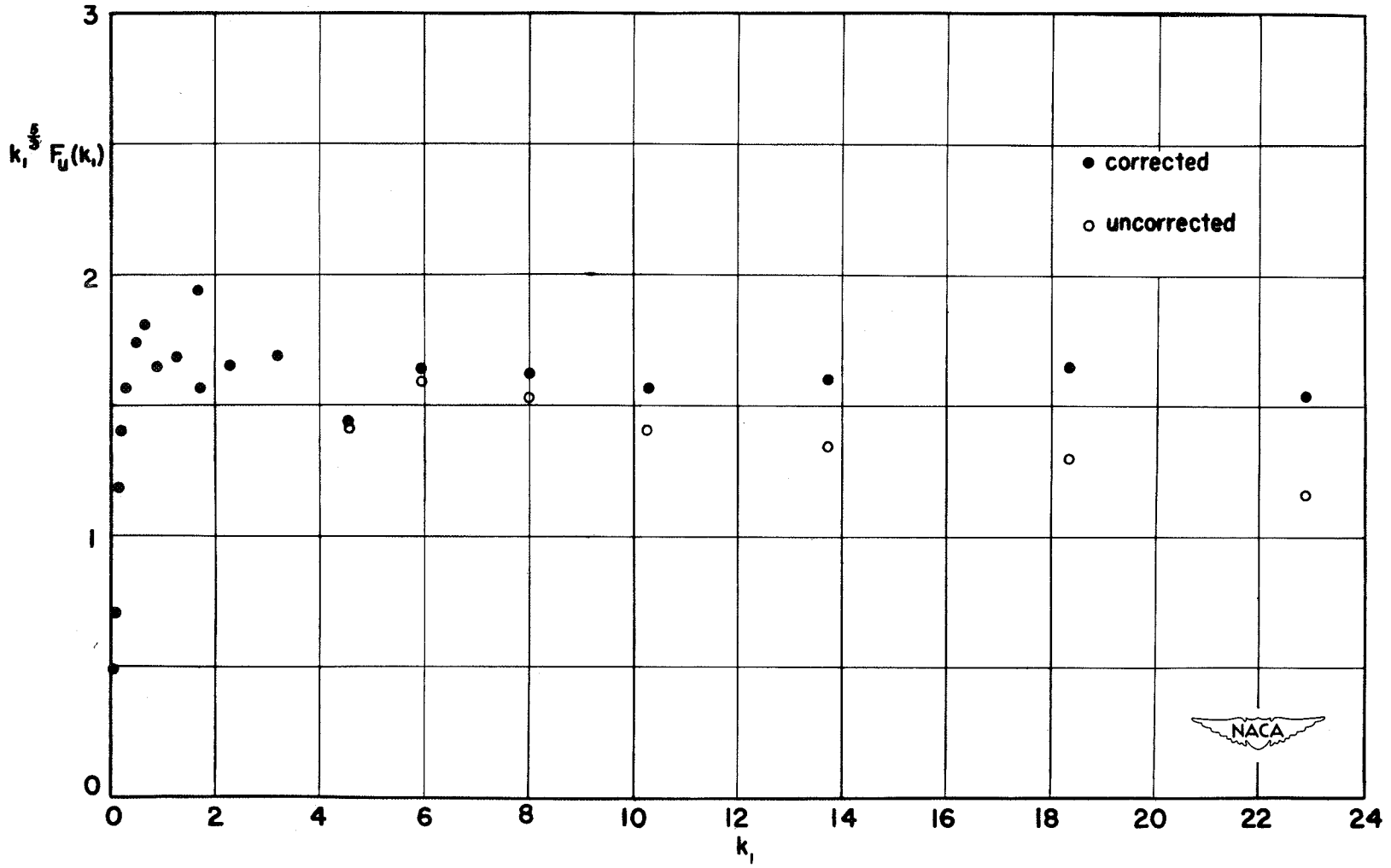


Figure 22.- Equilibrium range of  $u'$ -spectrum.  $R = 500,000$ ;  $r'/a = 0.28$ .

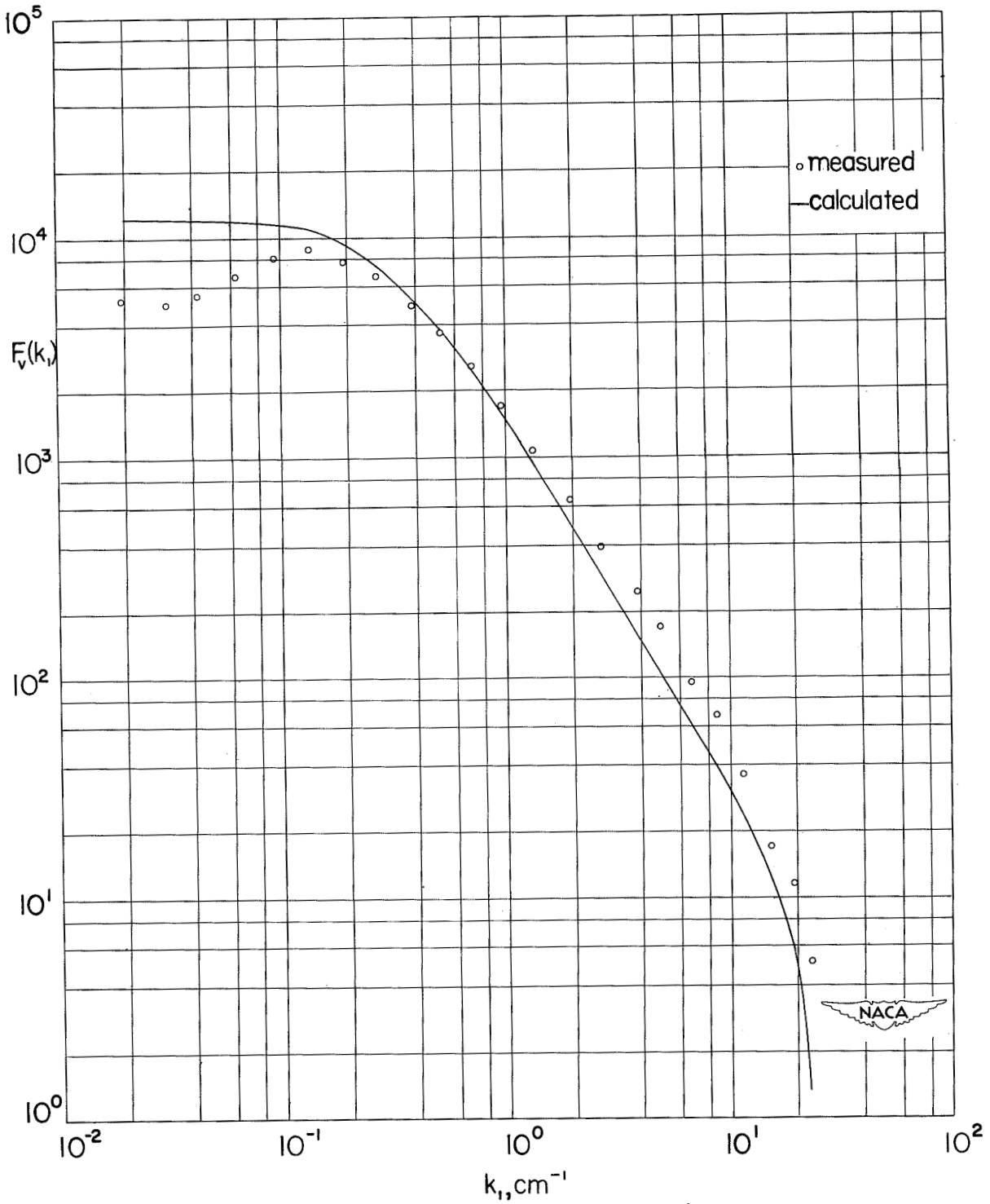


Figure 23.- Comparison of measured and calculated  $v'$ -spectrum.  $R = 500,000$ ;  
 $r'/a = 1.0$ .

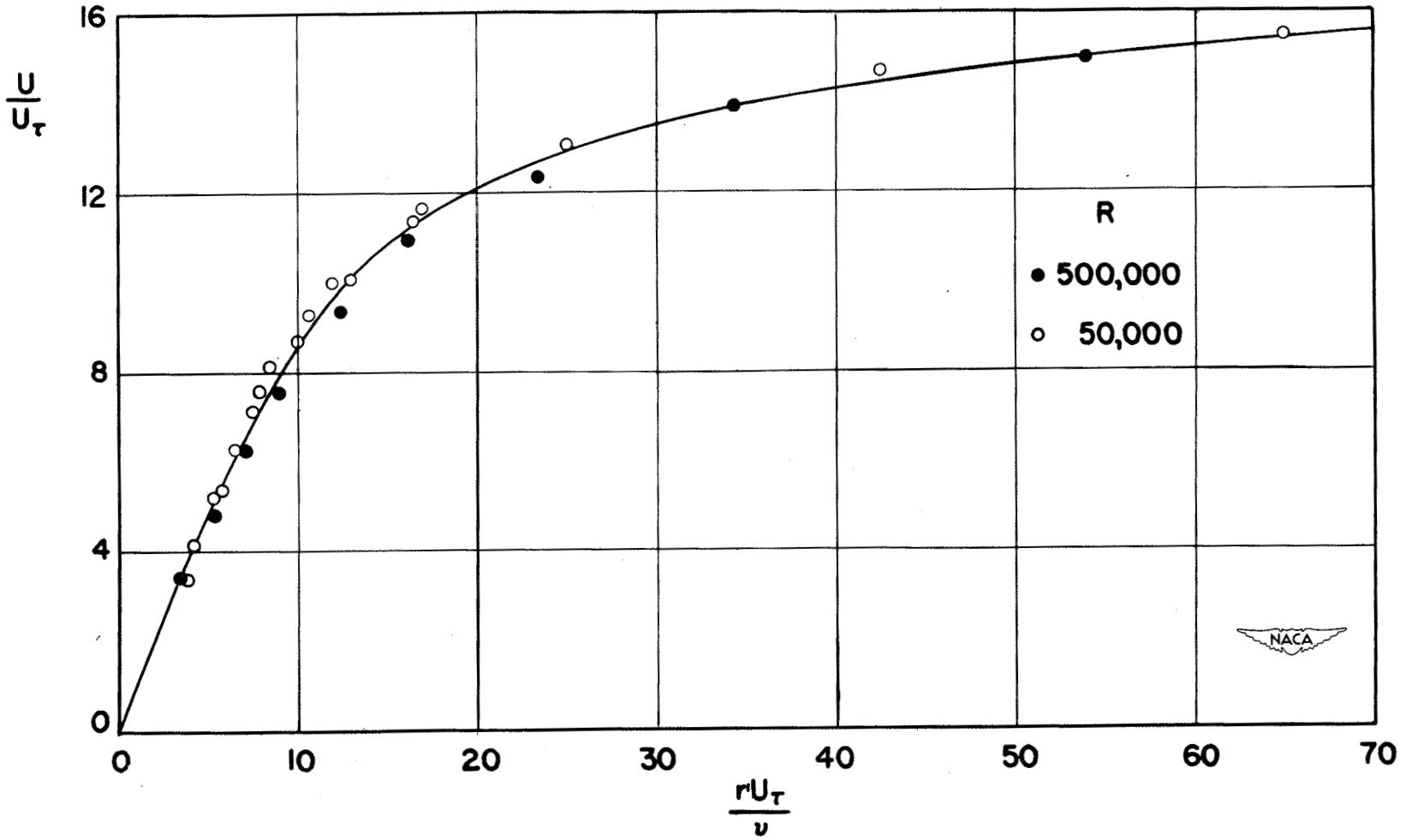


Figure 24.- Mean-velocity distribution near wall.

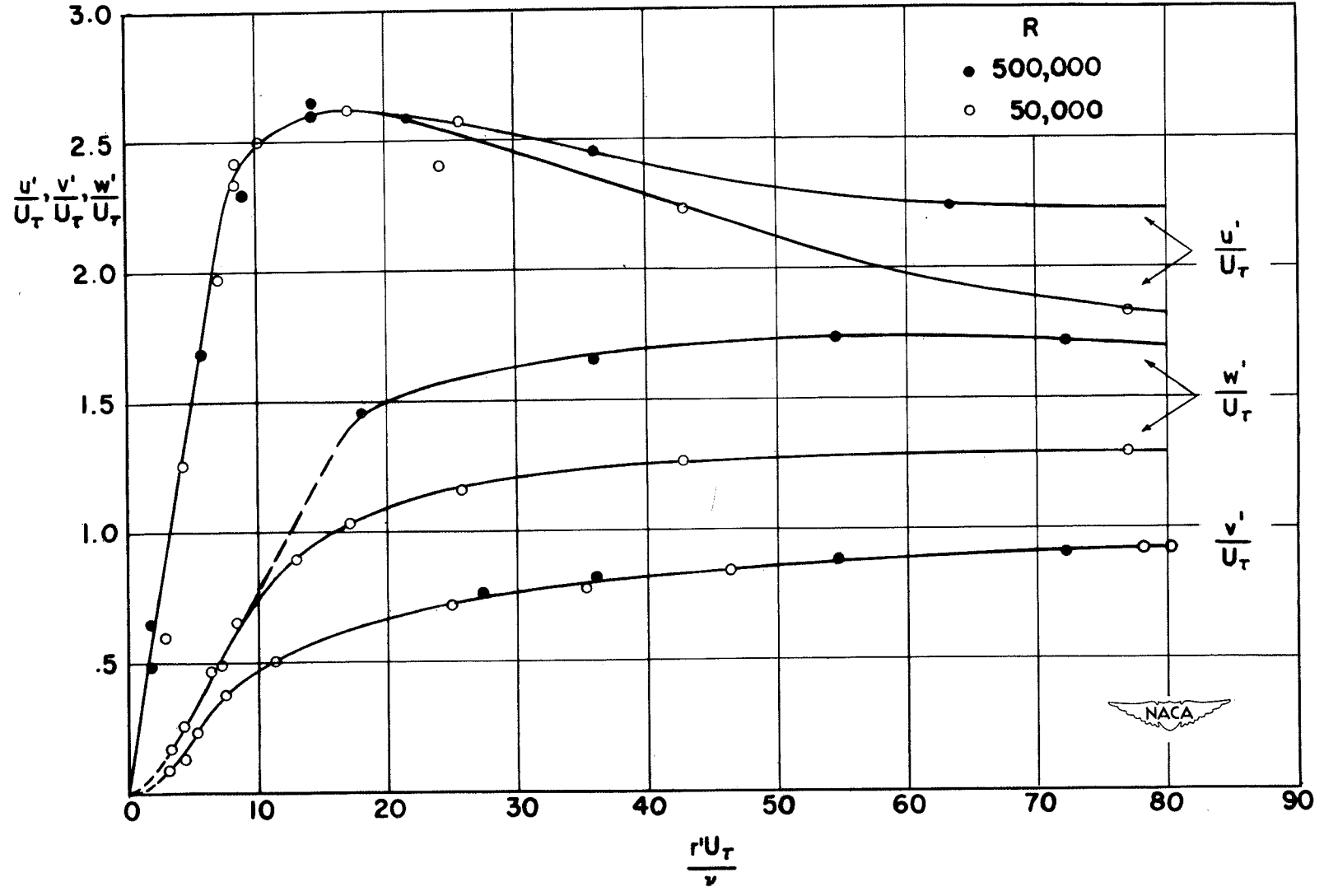


Figure 25.-  $u'$ ,  $v'$ , and  $w'$  distributions near wall.

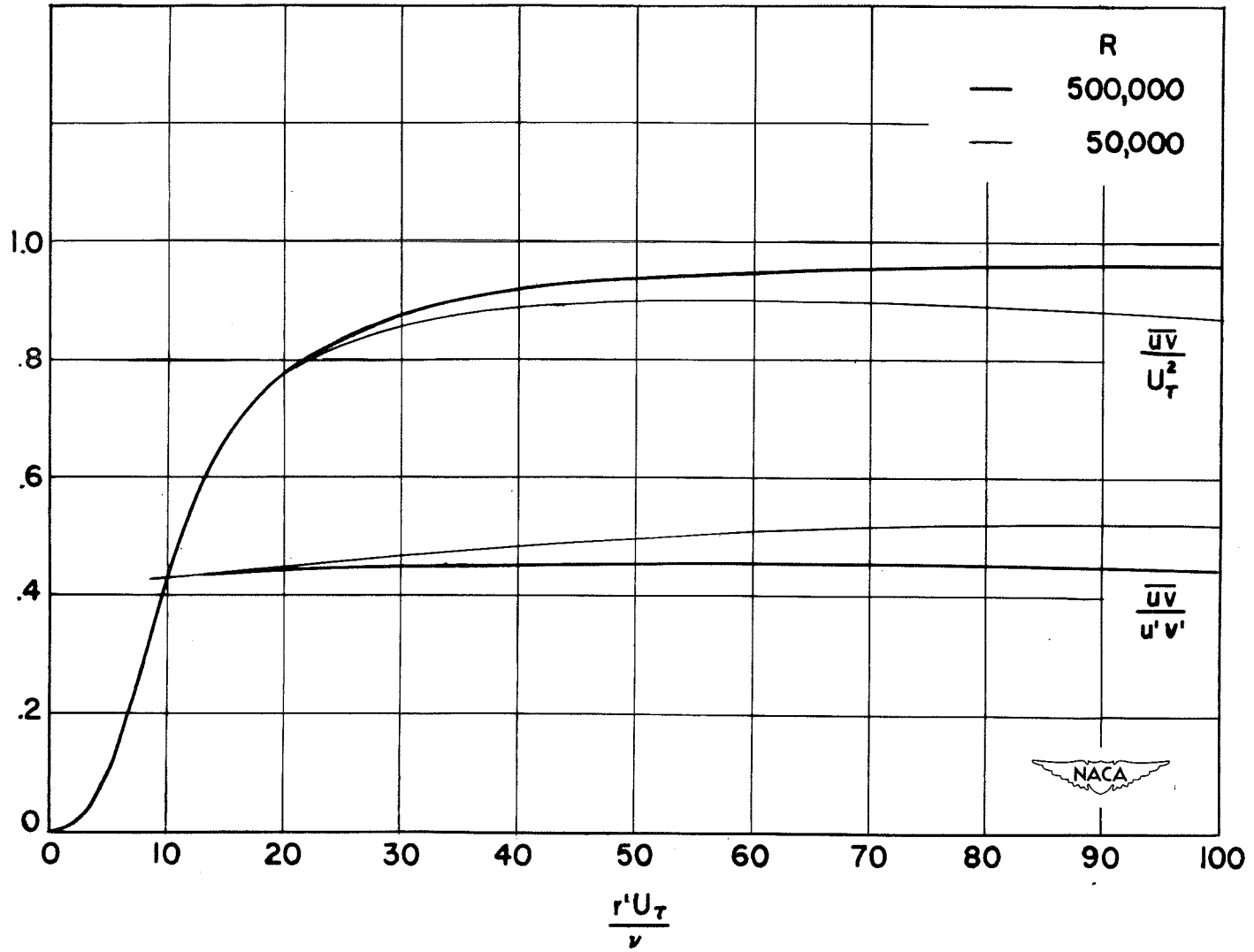


Figure 26.- Turbulent shearing stress and double-correlation coefficient near wall.